

# Accepted Manuscript

Novel c-Met inhibitory olive secoiridoid semisynthetic analogs for the control of invasive breast cancer

Mohamed M. Mohyeldin, Belnaser A. Busnena, Mohamed R. Akl, Ana Maria Dragoi, James A. Cardelli, Khalid A. El Sayed



PII: S0223-5234(16)30336-1

DOI: [10.1016/j.ejmech.2016.04.043](https://doi.org/10.1016/j.ejmech.2016.04.043)

Reference: EJMECH 8558

To appear in: *European Journal of Medicinal Chemistry*

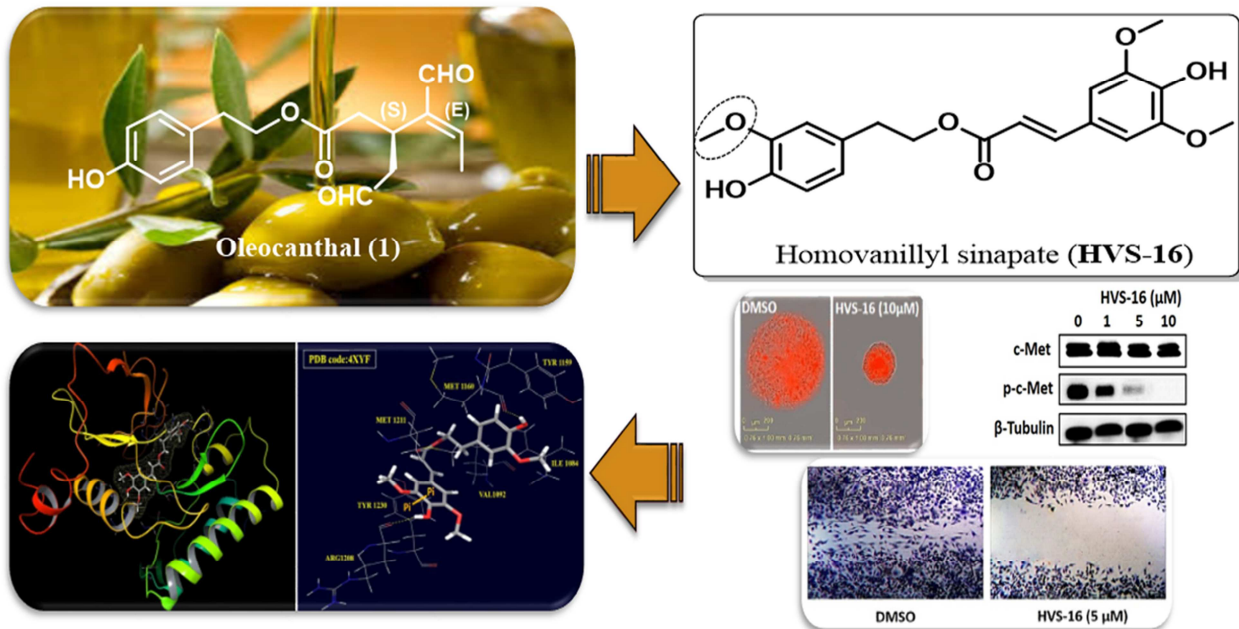
Received Date: 28 October 2015

Revised Date: 16 April 2016

Accepted Date: 16 April 2016

Please cite this article as: M.M. Mohyeldin, B.A. Busnena, M.R. Akl, A.M. Dragoi, J.A. Cardelli, K.A. El Sayed, Novel c-Met inhibitory olive secoiridoid semisynthetic analogs for the control of invasive breast cancer, *European Journal of Medicinal Chemistry* (2016), doi: 10.1016/j.ejmech.2016.04.043.

This is a PDF file of an unedited manuscript that has been accepted for publication. As a service to our customers we are providing this early version of the manuscript. The manuscript will undergo copyediting, typesetting, and review of the resulting proof before it is published in its final form. Please note that during the production process errors may be discovered which could affect the content, and all legal disclaimers that apply to the journal pertain.



**Novel c-Met Inhibitory Olive Secoiridoid Semisynthetic Analogs for the Control of  
Invasive Breast Cancer**

Mohamed M. Mohyeldin<sup>1</sup>, Belnaser A. Busnena<sup>1</sup>, Mohamed R. Akl<sup>1</sup>, Ana Maria Dragoi<sup>2</sup>, James  
A. Cardelli<sup>2</sup>, Khalid A. El Sayed<sup>1\*</sup>

<sup>1</sup>Department of Basic Pharmaceutical Sciences, School of Pharmacy, University of Louisiana at  
Monroe, 1800 Bienville Drive, Monroe, Louisiana 71201, USA

<sup>2</sup>Department of Microbiology and Feist-Weiller Cancer Center, Louisiana State University  
Health Sciences Center, Shreveport, Louisiana, USA

\* To whom Correspondence should be addressed. Telephone 318-342-1725.

Fax: 318-342-1737.

E-mail: [elsayed@ulm.edu](mailto:elsayed@ulm.edu)

## Abstract

Dysregulated receptor tyrosine kinase c-Met and its ligand HGF is valid and attractive molecular target for therapeutic blockade in cancer. Inspired by the chemical structure of the naturally occurring olive secoiridoid (-)-oleocanthal (**1**) and its documented anticancer activity against c-Met-dependent malignancies, a previous study reported tyrosol sinapate (**4**) as a c-Met inhibitor hit. This study reports additional semisynthetic optimization and SAR of **4** to improve its selective activity against c-Met-dependent breast cancer by increasing its capacity to inhibit c-Met phosphorylation. Forty-three compounds (**5-47**) were synthesized, among which the novel analog homovanillyl sinapate (**HVS-16**) was distinguished for its remarkable activity. **HVS-16** substantially impaired c-Met-mediated proliferation, migration, and invasion across human breast cancer cell lines in two- and three-dimensional culture systems, while similar treatment doses were found to have effect neither on the non-tumorigenic human mammary epithelial cell growth nor on the c-Met independent breast cancer cell viability. **HVS-16** showed a dose-dependent inhibition of ligand-mediated c-Met activation in human breast cancer cells. Docking studies revealed that **HVS-16** fits very well inside c-Met crystal structures, satisfying critical interactions at the ATP binding site. This study identified important structural pharmacophoric features in **HVS-16** and correlated its postulated binding pose with c-Met kinase assay data that would guide future olive secoiridoid bioisostere lead design. Results presented herein suggest **HVS-16** as a promising c-Met inhibitor validated hit with potential to control invasive breast malignancies with aberrant c-Met activity.

## Keywords

Antimigratory, Antiproliferative, Anti-invasive, Breast cancer, c-Met, Olive secoiridoids, Homovanillyl sinapate.

## 1. Introduction

c-Met is the prototypic member of a unique subfamily of receptor tyrosine kinases (RTKs) which also contains the protein kinase Ron. It is the only known high-affinity receptor for its ligand hepatocyte growth factor (HGF), also known as scatter factor [1]. Upon HGF stimulation, c-Met induces several biological responses including cell proliferation, survival, differentiation, motility, angiogenesis, and invasion [2, 3]. c-Met dysregulated activation is involved in the development and progression of multiple tumor types, such as hereditary papillary renal cell carcinoma [4], lung cancers [5], head and neck cancers [6], breast and prostate cancers [7, 8] as well as gastric cancer [9]. The overexpression of c-Met and/or HGF has been associated with a metastatic phenotype and poor prognosis in breast and gastric cancers [10, 11]. Activation of HGF/c-Met signaling in the tumor microenvironment may confer resistance to anti-RTK cancer therapies already in clinical use, including EGFR and BRAF anticancer kinase inhibitors [12, 13]. Given the important role of aberrant HGF/c-Met signaling in cancer progression and resistance to cancer therapies, this signaling axis has emerged as one of the most promising therapeutic targets in anticancer drug discovery [7]. Targeting the c-Met kinase domain with small molecules resulted in more than 240 c-Met inhibitors reaching various clinical stages as cancer treatments [14, 15]. Pfizer's c-Met/ALK dual inhibitor crizotinib and Exelixis' VEGFR2/c-Met multikinase inhibitor cabozantinib are the first small-molecule c-Met inhibitors approved so far by the FDA for the treatment of late-stage NSCLC and metastatic medullary thyroid cancer, respectively [15].

The Mediterranean populations have reduced risk incidence for particular types of cancer, compared to other geographical populations. This may be attributed to the Mediterranean diet rich in extra-virgin olive oil (EVOO), apart from possible genetic factors

[16]. EVOO is rich in other minor bioactive phenolics, including simple phenols, phenolic acids, flavonoids, lignans, and secoiridoids [17]. (-)-Oleocanthal (**1**) is a naturally occurring secoiridoid from EVOO, which has recently attracted considerable attention due to its various biological effects in inflammation, Alzheimer's disease and cancer [18-22]. (-)-Oleocanthal has been shown to mediate its anticancer effects through the disruption of c-Met kinase-related pathways [20, 23]. **1** Competitively inhibited the c-Met kinase activation in a biochemical assay [19, 20]. In addition, the intracellular mechanisms involved in mediating **1**'s c-Met-related anticancer effects in breast cancer cells and in a mouse model have been characterized [23]. Recently, **1** proved to target Hsp90, a chaperone protein stabilizing a number of proteins required for tumor growth, including c-Met [24]. Ligstroside aglycone (**2**) is another olive secoiridoid, which triggered apoptotic cell death in HER2-overexpressing breast carcinoma and showed moderate cytotoxicity against a panel of human cancer cell lines [25]. Unlike **1**, ligstroside aglycone did not demonstrate c-Met inhibition despite showing moderate antimigratory activity against human metastatic breast cancer cells [19].

Chemically, **1** is the elenolic acid ester of the common olive phenolic alcohol tyrosol (**3**). Based on the activity of **1** as c-Met inhibitor, the synthesis of different tyrosol ester and carbamate analogs was reported [19]. Design of these analogs was based on replacing the **1**'s elenolic acid moiety with different bioisosteres, including natural olive-derived phenolic acids, synthetic heteroaromatic acids, and diverse aromatic carbamates, to develop **1**-based c-Met inhibitors. Among these analogs, tyrosol sinapate (**4**) showed moderate ATP-competitive c-Met phosphorylation inhibitory activity in cell-free assays [19]. **4** Demonstrated antimigratory, antiproliferative, and anti-invasive activities against the highly metastatic human breast cancer MDA-MB-231 cells consistent with its c-Met inhibitory activity, without being toxic to the non-tumorigenic human mammary epithelial cells [19]. Therefore, the main objective of this study is

to subject the initial hit **4** to extensive structure-activity relationship (SAR) studies via optimization of its sinapic acid and tyrosol moieties as well as the ester linker.

## 2. Results and Discussion

### 2.1. Chemistry

Thirty-seven new **7-9**, **11-14** (Scheme 1), **16**, **18-39** and **41-47** (Scheme 2) and six known analogs **5**, **6**, **10**, **15** (Scheme 1), **17** and **40** (Scheme 2) were synthesized. The esters **5-9** and **13-47** have been prepared by convenient synthesis using the highly chemoselective Mitsunobu esterification reaction (Scheme SI1). Sinapic acid amidation reaction of tyramine has been used to synthesize analog **10** (Scheme SI2). Furthermore, condensation reaction of tyramine with sinapaldehyde has been used to generate the imine **11** (Scheme SI3). In a similar fashion, the 1,2,4-oxadiazole analog **12** has been synthesized via condensation reactions involving sinapic acid and hydroxyl-benzamidine oxime (Scheme SI4). Most reaction yields were in the range of 50-60%. Concerning the known analogs, tyrosol ferulate (**5**) was first isolated as a natural product from *Heracleum lanatum* Michx. in 1982 [26]. Tyrosol coumarate (**6**) was isolated from *Sargentodoxa cuneata* in 1988 [27]. Both **5** and **6** have shown weak cytotoxicity against the oral cancer cell lines SAS and OEC-M1 ( $IC_{50} > 100 \mu M$ ) [28]. Tyrosol sinapamide (**10**) was first isolated from the branches of *Porcelia macrocarpa* and showed moderate cytotoxicity against human myeloid leukemia HL-60 and cervical cancer HeLa cell lines [29-31]. Hydroxytyrosol ferulate (**15**) was patented in 2007 for dermatological care purpose [32]. Homovanillyl ferulate (**17**) has been only reported as a natural product from the wood of *Alnus hirsuta* in 1972 [33]. Finally, coniferyl ferulate (**40**) was isolated from the aerial parts of *Coreopsis longula* in 1985 [34]. Recently, **40** demonstrated a strong inhibition of human placental glutathione *S*-transferase (GST) activity, with an  $IC_{50}$  value of  $0.3 \mu M$ , and

therefore proposed as an antitumor adjuvant therapy to improve drug sensitization and reverse resistance [35]. Re-synthesizing these known compounds aimed to assess their c-Met inhibitory and anticancer activities against MDA-MB-231 cells. The identity of known compounds was confirmed by comparison of their  $^1\text{H}$  and  $^{13}\text{C}$  NMR data (Tables SI1-4, SI9, SI12-15 and SI20) with literature [26, 27, 31, 34].

The structures of the new compounds were confirmed by  $^1\text{H}$  NMR,  $^{13}\text{C}$  NMR, and MS spectra. For instance, the HRESIMS data of **7** showed a molecular ion peak at  $m/z$  345.1336  $[\text{M}-\text{H}]^-$ , suggesting a molecular formula  $\text{C}_{19}\text{H}_{22}\text{O}_6$  and possible ester analog of **3**.  $^1\text{H}$  and  $^{13}\text{C}$  NMR data indicated that **7** is 4-hydroxyphenethyl 3-(4-hydroxy-3,5-dimethoxyphenyl)propanoate (Tables SI1 and SI12). The  $^1\text{H}$  NMR and PENDANT data of **7** showed typical patterns of aromatic signals for *para*-substituted phenethyl moiety, in addition to aromatic and methoxy signals for the sinapinic acid moiety. The  $^1\text{H}$  NMR data of **7** also revealed the downfield shifting of the methylene  $\text{H}_{2-1'}$  to  $\delta_{\text{H}}$  4.24, compared to that of its parent tyrosol moiety **3** ( $\Delta\delta_{\text{H}}$  +0.54), suggesting possible esterification of the primary alcohol C-1' (Table SI1). Esterification was further confirmed in PENDANT spectrum through the characteristic downfield ester carbonyl C-1 ( $\delta_{\text{C}}$  173.1, Table SI12), in addition to the downfield shift of C-1' ( $\Delta\delta_{\text{C}}$  +4.20, Table SI12), and the upfield shift of C-2' ( $\Delta\delta_{\text{C}}$  -4.20). Additionally, esterification was supported by a  $^3\text{J}$ -HMBC correlation of the methylene triplet  $\text{H}_{2-1'}$  with the ester carbonyl C-1, confirming the identity of **7** as tyrosol sinapinate. The  $^1\text{H}$  and  $^{13}\text{C}$  NMR data of compounds **8-47** (Tables SI1-22) as well as their HRESIMS data were used to confirm their identity in a similar fashion.

## 2.2. Biological Evaluation and Structure-Activity Relationship (SAR)

### 2.2.1. Z'-LYTE™ c-Met kinase assay

The initial screening cascade used the Life Sciences' cell-free Z'-LYTE™ enzymatic assay as the screening assessment for designed compounds. Because all c-Met-mediated functions are dependent on its kinase activity [36], the in vitro ability of synthesized analogs **5-47** to inhibit c-Met phosphorylation (activation) was directly tested on the purified kinase domain of c-Met (amino acids 956–1390), that was in vitro phosphorylated to achieve the highest level of intrinsic kinase activity. In this experiment, Z'-LYTE™ Tyr6 peptide was used as a substrate; thus, the changes in its phosphorylation can directly reflect the c-Met kinase activity. Meanwhile, **1** and **4** were used as positive controls for activity comparison. Table 1 shows the concentration that resulted in 50% c-Met phosphorylation inhibition (IC<sub>50</sub> values) for all compounds. The calculated IC<sub>50</sub> of **1** in this assay was 5.2 μM, which was consistent with its reported value 4.8 μM, validating the results of this study [19, 20]. The SAR study was based upon investigating three moieties of the preliminary hit **4**; the sinapic acid and tyrosol moieties and their ester linker. The SAR study started with exploring the importance of methoxy groups in the sinapic acid moiety of **4** for c-Met inhibition by synthesizing analogs **5** and **6**. Tyrosol ferulate (**5**) has only one methoxy substituent in *ortho*-position to the C-7 phenolic hydroxyl group. Analog **5** was able to inhibit c-Met kinase phosphorylation by nearly the same extent as the parent tyrosol sinapate (**4**) with an IC<sub>50</sub> value of 12.9 μM. However, omitting both **4**'s methoxy groups, as represented by tyrosol coumarate (**6**) significantly reduced the activity to an IC<sub>50</sub> value of 20.2 μM (Table 1). Therefore, the presence of at least one methoxy group next to the phenolic hydroxyl in the acid part of **4** is essential for the kinase inhibitory activity. The importance of the free C-7 phenolic hydroxyl group for c-Met inhibition was previously investigated via the remarkable activity difference between **4** and its C-7 methyl ether, which highlighted the hydrogen bond donating role (HBD) of the acid part's phenolic hydroxyl for binding [19]. Bioisosteric replacement of this group with an amino group did not show a

significant improvement in the activity as represented by analog **38**, which has an IC<sub>50</sub> value of 12.2  $\mu$ M, suggesting the need for only one HBD group at the C-7 position for best c-Met binding (Table 1). Reducing the sinapic acid's double bond  $\Delta^{2,3}$  in **4**, as in analog **7**, abolished the kinase inhibitory activity. Similarly, substituting the  $\alpha$ -carbon of the olefinic double bond with cyano or sulfhydryl groups significantly reduced the activity as in analogs **8** and **9**. The influence of changing the geometrical isomerism (*E/Z* isomers) around the olefinic  $\Delta^{2,3}$  has been also studied through the synthesis of the *Z*-analogs **34** and **36** and comparing their c-Met inhibitory activities with the corresponding *E*-analogs **33** and **35** (Table 1). The *E*-isomer, in all analogs, proved to be significantly more potent at the ATP binding pocket of c-Met compared to the *Z*-isomer, which clearly indicated that the c-Met inhibitory activity of this class resides in the *E*-isomer. Concerning the ester linker, ester analogs of **3** were previously shown to be more active than carbamate and sulfonyl carbamate analogs, suggesting the preference of the ester pharmacophore for better c-Met inhibitory activity [19]. However, the critical role of the ester functionality in **4** has been further explored by using different bioisosteres, including the amide **10**, the imine **11**, and the 1,2,4-oxadiazole moiety **12**. The lack of c-Met kinase inhibitory activity of **10-12** confirmed the important role of the ester functionality at the ATP binding pocket (Table 1). The ester moiety was hypothesized not to contribute any binding role, based on previous findings, yet it provided the proper molecular size and conformation for adequate binding [19, 20]. The ester linker must have been required to maintain the bioactive U-shaped binding mode at the Met's ATP binding pocket characteristic for type-I binding and thus, it is indispensable for the activity. Therefore, ferulic and/or sinapic acid moieties were maintained as appropriate scaffolds for c-Met inhibition while optimizing the alcohol part. The alcohol moiety optimization began with determining the activity role of the tyrosol's C-6' phenolic hydroxyl group of **4** via its bioisosteric replacement with an amino group in analogs **18** and **19** and with a

methoxy group in analogs **24** and **26**. Compounds **18** and **19** exhibited more than 2-fold increase in the c-Met kinase inhibitory activity versus **4**, with  $IC_{50}$  values of 5.2 and 6.1  $\mu M$ , respectively. On the other hand, replacing the C-6' phenolic hydroxyl group with a methoxy group in **24** and **26** caused a drastic reduction in the activity, with  $IC_{50} > 20.0 \mu M$  (Table 1). This clearly highlighted the importance of the HBD role of C-6' phenolic hydroxyl group in **4** for maintaining potency, and suggests that an additional HBD at this position, as represented by an amino group, may offer better binding affinity at the ATP binding pocket, improving the overall bioactivity. This finding augmented previous preliminary binding mode study of **4** in three highly resolved c-Met kinase domain crystal structures where the tyrosol's C-6' phenolic hydroxyl group exhibited HBD interactions with the hinge region's essential amino acids Met1160 or Pro1158 of the three c-Met crystal structures [19]. The chain extension/shortening as a classical medicinal chemistry optimization strategy was adopted in order to investigate the optimal length of the alkyl side chain linker in the tyrosol moiety of **4** for efficient c-Met inhibition. Increasing the chain length by one carbon atom, as represented by analogs **20**, **21**, and **35** showed a slight improvement in the c-Met inhibitory activity compared to **4**, with  $IC_{50}$  values of 8.2, 9.1 and 8.0  $\mu M$ , respectively (Table 1). Decreasing the length of the alkyl side chain linker by one carbon atom, as represented by analog **32**, demonstrated a nearly similar pattern of activity enhancement, with an  $IC_{50}$  value of 8.3  $\mu M$  (Table 1). However, shortening the chain length by an additional carbon atom represented by analogs **22** and **23** completely diminished the c-Met inhibitory activity (Table 1). This clearly indicates the important role of the distance limit between the two aromatic rings A and B of the alcohol and the acid moieties for optimal c-Met inhibition. The results suggested that retaining six to eight chemical bonds i.e. five to seven atoms in the linker could afford a proper spatial distance between the phenyl rings A and B and thus maintain the c-Met inhibition. Based on these results, 4-hydroxybenzyl

alcohol and 3-(4-hydroxyphenyl)-1-propanol in addition to tyrosol were considered as potential scaffolds appropriate for further optimization of the alcohol moiety. In order to explore the effect of replacing the tyrosol's phenolic hydroxyl group with a catechol, the common olive phenolic hydroxytyrosol was used in the esterification reactions, as represented by analogs **13**-**15** and **37**. Replacing the tyrosol moiety in **4**, **5** and **38** with hydroxytyrosol, as shown in analogs **13**, **15** and **37**, improved the c-Met inhibitory activity by at least 2-folds, demonstrating IC<sub>50</sub> values of 5.8, 7.8 and 6.9 μM, respectively (Table 1). The binding role of this C-5' phenolic hydroxyl group was investigated by replacing it with an amino group as in analog **28**. Surprisingly, **28** was much less active (~2-fold) than **13**, with an IC<sub>50</sub> value of 11.4 μM, suggesting no HBD role for C-5' OH in **13** for the c-Met inhibition (Table 1). Instead, C-5' oxygen in **13** is likely to play a better hydrogen bond acceptor (HBA) role for c-Met binding when compared to the aniline nitrogen in **28**. The lone pair of the **28**'s nitrogen atom can interact with the neighboring π-system of the benzene ring to form various resonance structures and hence it is less likely to take part in a hydrogen bond (HB). In contrast, the C-5' oxygen in **13** has an additional lone pair of electrons which are not involved in resonance and more likely to play a significant HBA role at the ATP binding pocket, improving the overall activity as compared to **28**. In order to gain further insight on this position, the C-5' phenolic hydroxyl group in **13**, **15** and **37** was replaced with a methoxy group in analogs **16**, **17** and **33**. Interestingly, these analogs exhibited nearly six-fold enhancement in the c-Met kinase inhibitory activity, with IC<sub>50</sub> values of 1.0, 1.3 and 1.2 μM, respectively (Table 1, Figure 1). This clearly indicated the preference of a small hydrophobic methoxy group, retaining the HBA property, over the C-5' phenolic hydroxyl group in ring A. The binding affinity enhancement of **16**, **17** and **33** might be attributed to the ability of the C-5' methoxy group to exert hydrophobic interactions at the ATP binding site of the c-Met protein, since both the methoxy and hydroxyl

can act as HBA groups but the superior activity of the methoxy group at this position suggested additional hydrophobic interactions with the c-Met kinase. Subsequently, a strategy of adding a methoxy group at the same position, next to the phenolic hydroxyl group, in both 4-hydroxybenzyl alcohol and 3-(4-hydroxyphenyl)-1-propanol was adopted to probe possible activity improvement. Accordingly, 3-(4-hydroxyphenyl)-1-propanol was replaced with 4-(3-hydroxypropyl)-2-methoxyphenol in the esterification reactions as represented by analogs **29** and **30**. Adding a methoxy group in **29** and **30** did not improve the activity as would have been expected, compared to the unsubstituted analogs **20** and **21** (Table 1). This might be due to the involvement of the methoxy group in unfavorable interaction(s) or steric clashes with the target receptor or its inability to demonstrate good fitting within the hydrophobic space as a result of the alkyl side chain elongation by one carbon atom. In order to solve this problem, a structural rigidification strategy, via introducing a double bond in the alkyl side chain of the alcohol part, was adopted to confer a favorable effect on the entropic ( $\Delta S$ ) component of the binding affinity without adversely affecting the enthalpy ( $\Delta H$ ) component, if nearly the correct conformer can be locked at the ATP binding pocket via this strategy. However, this approach was not successful, as the  $\Delta^{2',3'}$  unsaturation in the alkyl side chain of 4-(3-hydroxypropyl)-2-methoxyphenol totally eliminated the activity, as seen in analogs **31** and **40** (Table 1). Encouraged by the promising c-Met inhibitory activity of analog **32**, compared to the parent **4**, a methoxy group was sought to be placed next to the phenolic OH in ring A to gain potency, which afforded compound **41**. The methoxy substitution only resulted in approximately 4-fold increase in the activity with the 5-atom linker between the phenyl rings A and B (**41** versus **32**) compared to a 14-fold enhancement in the potency for the 6-atom linker (**16** versus **4**, Table 1). A possible explanation could be that the five-atom linker is neither enough to provide the optimal distance to form an intermolecular HB from a probable donor amino acid in the ATP

binding pocket to the C-4'-OCH<sub>3</sub> in **41** nor to perfectly accommodate this methoxy into the hydrophobic space of c-Met kinase. Hence, the 6-atom linker provided by the 2-phenylethanol (tyrosol) ester series was optimum and might furnish novel promising c-Met inhibitors. Therefore, the active homovanillyl alcohol moiety in **16** was maintained and an additional substitution with a methoxy group at C-7' position of the phenyl ring A was attempted. However, the additional C-7'-OCH<sub>3</sub> substituent in **42** and **43** significantly eroded the potency, resulting in a 3-fold loss of activity when compared to **16** and **17** (Table 1). This might be due to a steric factor at the C-7' position or the involvement of the methoxy group in unfavorable interaction(s) with the target receptor. At this point, the PDB deposited crystal structure of crizotinib (PDB code: 2WGJ) was obtained as an ATP-competitive c-Met inhibitor [37]. Crizotinib structure (**48**) was analyzed and identified its 2-aminopyridine moiety bound to the c-Met's hinge region via HB interaction of the pyridine nitrogen with the Met1160 amide NH. On the basis of this observation, a strategy of pharmacophore hybridization was adopted in an attempt to gain potency via introducing the typical kinase hinge binding aminopyridyl group, similar to that of **48**, to the six-atom and five-atom linker pharmacophores as represented by analogs **44-47**. Interestingly, compounds **44** and **45**, with six-atom linker, were almost equipotent to **16** and **17**, against c-Met kinase enzyme, respectively, suggesting the ability of the 2-aminopyridine moiety to make up for the lost activity due to the absence of small hydrophobic methoxy group at C-5' in the pyridyl moiety, possibly by offering additional binding pharmacophore, C-6' amino group, in addition to the electron-poor pyridine ring which might be advantageous to the potency (Table 1). On the other hand, the five-atom linker analogs **46** and **47** were less active (>2-folds) than **39** and **41**, with IC<sub>50</sub> values of 5.8 and 5.3 μM, respectively (Table 1). This could be attributed to the inability of the five-atom linker to provide the optimal distance to form an intermolecular HB between the ATP binding pocket amino

acids with the amino pyridine nucleus of **46** and **47**, along with the lack of potential hydrophobic interactions due to the absence of C-5' methoxy group and thus negatively influencing the activity. Taken together, the SAR presented herein afforded nine analogs (**16**, **17**, **33**, **39**, and **41-45**) with better c-Met inhibitory activity than oleocanthal (**1**, Figure 1, Table 1). Apparently, **HVS-16** proved to be the most potent inhibitor in this cell-free assay, being able to inhibit c-Met phosphorylation induced by the addition of ATP in a dose-dependent manner and demonstrating nearly fourteen-fold enhancement in the activity versus the parent **4** and five-fold activity improvement compared to **1** (Figure 1, Table 1). Thus, **HVS-16** can be considered as a potential c-Met inhibitor hit appropriate for further validation.

### 2.2.2. HGF-induced cell proliferation MTT assay

The growth inhibitory effect of analogs **1-47** on the c-Met-dependent, triple negative human breast carcinoma (TNBC) MDA-MB-231 and MDA-MB-468 cells was assessed using MTT assay. HGF (40 ng/mL) was used in the growth media as a mitogen to induce cell proliferation through activating the c-Met receptor. In this assay, at least four different concentrations per each analog were tested and used to assess the concentration that resulted in 50% cell growth inhibition ( $IC_{50}$ ) (Table 2). Oleocanthal (**1**) and tyrosol sinapate (**4**) were used as standard positive controls. The parent **4** as well as the natural olive phenolics **2** and **3** showed moderate to high micromolar antiproliferative activity against both breast cancer cell lines (Table 2). In general, nearly all olive secoiridoid semisynthetic bioisosteres demonstrated better antiproliferative activity than the parent **4** as well as the natural phenolics **2** and **3**, highlighting not only the importance of the moieties of tested analogs that belong to acids and alcohols used for the activity, compared to **3**, but also the significance of introducing particular substituents at the two aromatic rings A and B of the alcohol and the acid moieties, compared to **4**, as well as

the impact of optimizing the distance limit between these two rings. The antiproliferative activity level of all synthesized analogs towards MDA-MB-468 cell line is parallel to the one observed for MDA-MB-231 cells and thus the discussion mainly focused on the latter cell line. Analogs **16**, **20**, **21**, **24-26**, **28**, **37**, **39**, **41**, **44** and **45** showed the most promising antiproliferative activity in this assay with  $IC_{50}$  values  $<10 \mu M$  (Table 2). Obviously, **21**, **39** and **41** were among the most active compounds, inhibiting cell viability with  $IC_{50}$  values of 4.4, 4.2 and 6.3  $\mu M$ , respectively, and demonstrating thirteen to nineteen-fold enhancement in the activity, compared to **4** ( $IC_{50}$  79.5  $\mu M$ ) and more than two to four-fold improvement versus **1** ( $IC_{50}$  15  $\mu M$ , Table 2, Figure 2). This clearly indicates the significant impact of extending the tyrosol alkyl side chain linker in **21** as well as chain shortening in **39** and **41** on improving the antiproliferative activity. **HVS-16**, the most potent c-Met phosphorylation inhibitor in the Z-LYTE™ assay, was also the most active analog in cell proliferation assay. **HVS-16** significantly inhibited MDA-MB-231 and MDA-MB-468 cell growth in a dose-dependent manner as compared to vehicle-treated cells, with  $IC_{50}$  values of 3.8 and 6  $\mu M$ , respectively, exhibiting nearly twenty-one-fold improvement in the antiproliferative activity versus **4**, parallel to its c-Met kinase inhibitory potential (Table 2). Generally, the antiproliferative SAR observed in this assay is parallel to the one discussed above for the c-Met inhibitory activity in the Z-LYTE™ kinase assay, with only few exceptions to be addressed. Firstly, although the semisynthetic esters **39** and **41** were almost equipotent to **HVS-16** in cell proliferation assay, they were 2-fold less active than **HVS-16** in the Z-LYTE™ kinase assay suggesting other molecular target(s), in addition to c-Met, for their antiproliferative activity (Tables 1 and 2). Secondly, analogs **20** and **21** were active against the breast cancer MDA-MB-231 cells, with  $IC_{50}$  values of 7.6 and 4.4  $\mu M$ , respectively, whereas only marginally active against c-Met in the Z-LYTE™ assay, with  $IC_{50}$  values of 8.2 and 9.1  $\mu M$ , respectively (Tables 1 and 2). This

clearly indicates that the chain extension strategy adopted in **20** and **21** was able to improve the antiproliferative activity, only partially through inhibition of c-Met activation. A possible explanation could be that alkyl side chain elongation by an additional carbon might allow the phenyl ring A of the alcohol moiety to be involved in  $\pi$ - $\pi$  stacking with a molecular target receptor other than c-Met, thus anchoring the molecule in a pose that allows for better ligand-receptor interaction, and hence better antiproliferative activity. Similarly, analog **28**, with an amino group at the C-5' of the alcohol part, was only 2-fold less potent than **HVS-16** in cell proliferation assay, with an  $IC_{50}$  value of 8.6  $\mu$ M, while being much less active (~11-folds) than **HVS-16** against c-Met in the kinase assay, with an  $IC_{50}$  value of 11.4  $\mu$ M (Tables 1 and 2). This may suggest the ability of the C-5' amino group of **28** to demonstrate strong HB interactions to molecular target(s) involved in cell proliferation, other than c-Met, offering better binding affinity and improving the overall activity of this compound in cell proliferation. Finally, despite the fact that replacing the C-6' phenolic hydroxyl group of the tyrosol part with a methoxy group as well as changing the geometrical isomerism (*E/Z* isomers) around the olefinic double bond of the acid part proved detrimental to c-Met inhibitory activity in the Z-LYTE™ assay, the semisynthetic esters **24-26** were still able to demonstrate promising antiproliferative activity against MDA-MB-231 cells, with  $IC_{50}$  values of 7.3, 8.2 and 9.2  $\mu$ M, respectively, suggesting molecular target(s) different from c-Met for their antiproliferative activity (Table 2). The effect of various doses of **21**, **39**, and **41** on the viability of MDA-MB-231 cells after 72 h culture period is demonstrated in Figure 2.

### 2.2.3. HGF-induced cell migration assay

Activation of the HGF/c-Met axis promotes cell migration, which contribute to the metastatic characteristics of malignant cells [23]. The in vitro wound-healing assay (WHA) is a

simple method to study directional cell migration in two dimensions [23, 38]. Thus, compounds **1-47** were evaluated for their antimigratory effect in the scratch WHA using the highly metastatic MDA-MB-231 cells. HGF (40 ng/mL) was used as a mitogen to induce cell migration via c-Met activation. The parent **4** and the natural phenolics **2** and **3** showed moderate to high  $\mu\text{M}$  antimigratory activity (Table 2). Generally, all semisynthetic analogs excluding **5**, **7**, **8**, **10** and **34** showed better antimigratory activity than their parent **4** (Table 2). Compared to their effect on cell proliferation, nearly all compounds were more potent as MDA-MB-231 cell migration inhibitors, with most analogs showing  $\text{IC}_{50}$  values  $<15 \mu\text{M}$  (Table 2). Compounds **11**, **13**, **15-17**, **20**, **21**, **33**, **35**, **37**, **39**, **44** and **45** showed the most promising antimigratory activity with  $\text{IC}_{50}$  values  $<5 \mu\text{M}$  (Table 2). Figure 3A shows the effect of the most active analogs **HVS-16**, **44** and **45** on cell migration across the wound inflicted in the MDA-MB-231 cell monolayer compared to the vehicle control as well as  $10 \mu\text{M}$  dose of **1** and  $20 \mu\text{M}$  dose of **4** as positive controls [19]. Apparently, **HVS-16** was the most active compound, significantly suppressing HGF-induced cell migration in a dose-dependent manner with an  $\text{IC}_{50}$  value of  $2.5 \mu\text{M}$ , demonstrating thirteen-fold enhancement in the activity, compared to **4** ( $\text{IC}_{50}$   $33.5 \mu\text{M}$ ) and three-fold improvement versus **1** ( $\text{IC}_{50}$   $7.5 \mu\text{M}$ ) (Table 2, Figure 3). It is interesting to note that **HVS-16** was the most active c-Met phosphorylation inhibitor in the Z-LYTE™ assay, suggesting a strong correlation between the results of both assays. Similarly, analogs **17**, **33**, **44** and **45** were able to inhibit cell migration with  $\text{IC}_{50}$  values of 4.6, 4.1, 3.6 and  $3.9 \mu\text{M}$ , respectively, parallel to their c-Met kinase inhibitory activities (Table 2, Figure 3). However, there was an exception related to the C-5' substitution at the phenyl ring A with HBD substituents in analogs **13**, **15**, **28** and **37**. Compounds **13**, **15** and **37**, with C-5' hydroxyl substituent, demonstrated comparable antimigratory activities to **17** and **33**, with  $\text{IC}_{50}$  values of 4.2, 4.5 and  $4.6 \mu\text{M}$ , respectively, while being five to seven-fold less active than **17** and **33**

against c-Met in the kinase assay (Tables 1 and 2). Additionally, analog **28**, with C-5' amino substituent, was still able to show promising antimigratory activity, with an IC<sub>50</sub> value of 5.2 μM, despite being nine-fold less active than **17** in the Z-LYTE™ assay (Tables 1 and 2). This illustrates the important role of the HBD substituents at C-5' position for optimal antimigratory activity, but only marginally through inhibition of c-Met activation. In a similar fashion, analogs **20**, **21** and **35** were almost equipotent to **33** in the WHA, with IC<sub>50</sub> values of 4.8, 4.1 and 4.3 μM, respectively, while being much less active (~8-fold) than **33** in the kinase assay (Tables 1 and 2). Therefore, analogous to cell proliferation, the chain extension in these analogs maintained the antimigratory activity, in spite of the significant drop in c-Met phosphorylation inhibition, compared to **33**. A significant difference in the antimigratory activity between **33** versus **34** was observed upon changing the acid part's Δ<sup>2,3</sup> geometry (*E/Z* isomers), consistent with the results of the Z-LYTE™ assay (Tables 1 and 2). However, changing the geometry in analogs with 7-atom linker between the phenyl rings A and B (**35** versus **36**) did not exhibit the same drop in antimigratory activity similar to that observed in the 6-atom linker analogs (**33** versus **34**) (Table 2). This clearly augmented our earlier observation that different molecular targets, other than c-Met, are dictating the migratory potential of these semisynthetic esters with 7-atom linker. In contrast, the 5-atom linker analogs **39** and **41** were 2-fold less active than **HVS-16** in WHA, with IC<sub>50</sub> values of 4.0 and 5.4 μM, respectively, parallel to their c-Met kinase inhibitory activities (Table 2). Surprisingly, the imine **11** and the 1,2,4-oxadiazole analog **12** were active in this cell migration assay, with IC<sub>50</sub> values of 4.6 and 16.3 μM, respectively, whereas were nearly inactive in both Z-LYTE™ and cell proliferation assays (Tables 1 and 2). Compounds **11** and **12** appeared to enhance only the antimigratory activity, compared to the parent analog **4**, by offering better binding affinity to migration targets, other than c-Met, and hence, improving the overall activity. Meanwhile, analogs **14**, **22-27**, **31** and **40** demonstrated

promising antimigratory activities, with almost no corresponding c-Met inhibitory potential in the kinase assay, suggesting other molecular target(s) for their antimigratory activity (Table 2).

#### 2.2.4. HGF-induced cell invasion assay

During the complicated process of cancer metastasis, the invasion of cancer cells is among the most important and serious steps. The new **HVS-16**, **21** and **39**, in addition to the parent **4**, were further evaluated for their ability to inhibit the invasiveness of the aggressive MDA-MB-231 cells using the Cultrex<sup>®</sup> BME cell invasion assay (Table 3, Figure 4) [38, 39]. Oleocanthol (**1**) was used as a positive control and its IC<sub>50</sub> was calculated for activity comparison (Table 3). HGF (40 ng/mL) was used as a mitogen to induce cell invasion via c-Met activation. Compound selection for testing in this assay was based on the overall performance in previous assays. **HVS-16** was the most active in Z-LYTE<sup>™</sup> as well as cell proliferation and migration assays while analogs **21** and **39** were among the most potent in cell proliferation and migration assays (Tables 1 and 2). The three analogs also demonstrated varying activity levels of c-Met inhibition in the cell-free assay, so that a strong correlation between their anti-invasive and c-Met inhibitory activities can be established (Table 1). Four different subtoxic concentrations (1, 5, 10 and 20  $\mu$ M) per each analog were tested and used to determine IC<sub>50</sub> values (Table 3, Figure 4). The parent **4** showed moderate  $\mu$ M anti-invasive activity, with an IC<sub>50</sub> value of 19.8  $\mu$ M (Table 3). Generally, the three tested analogs **HVS-16**, **21**, and **39** demonstrated better anti-invasive activity profile than their parents **1** and **4** (Table 3, Figure 4). This clearly highlighted the significance of introducing small hydrophobic methoxy substituents, retaining the HBA property, at the aromatic ring A in **HVS-16** and **39**, compared to **4**, and the impact of optimizing the distance limit between the aromatic rings A and B, as represented by **21** and **39**. **HVS-16** was the most active hit, significantly and dose-dependently

decreasing the level of HGF-mediated cell invasion, with an  $IC_{50}$  value of 2.7  $\mu$ M. **HVS-16** demonstrated seven-fold enhancement in anti-invasive activity, compared to **1** and **4**, parallel to its c-Met inhibitory activity (Table 3, Figure 4). Analog **39** was 3-fold less active than **HVS-16** in cell invasion assay, with an  $IC_{50}$  value of 7.1  $\mu$ M, consistent with their activity levels in the c-Met kinase assay (Table 3, Figure 4). Similarly, **21** exhibited a slight improvement in the anti-invasive activity compared to **4**, with an  $IC_{50}$  value of 14.2  $\mu$ M, perfectly matching its c-Met inhibitory activity (Table 3, Figure 4). There is an obvious strong correlation between the results of both Z-LYTE™ and cell invasion assays, reinforcing the hypothesis that c-Met is the primary target for the anti-invasive effects of these tested analogs.

#### ***2.2.5. HGF-induced 3D spheroid disaggregation model***

It is well-known that cultures grown as 3D spheroids more accurately mimic the natural tumor microenvironment and thus, more closely recapitulate the in vivo response to drugs, compared to the traditional 2D monolayer cultures [40]. Therefore, the aim of this study was to characterize the effects of **HVS-16**, **39**, and **41** on an implemented 3D spheroid culture of the breast cancer cell line MDA-MB-231, stimulated with HGF, in an attempt to assess its in vitro sensitivity to these analogs versus tumor cells grown as 2D monolayer cultures, which might give a better prediction of the in vivo profile of this class of compounds. After spheroid formation, the drug responsiveness was evaluated by measuring the extent of spheroid growth in response to either DMSO as vehicle control or increasing concentrations of **HVS-16** (1, 3 and 10  $\mu$ M) or a single dose of either **39** or **41** (10  $\mu$ M), for a treatment period of 72 h. Additionally, **1** has been tested at 20  $\mu$ M for activity comparison. Images were captured every 4 h using the Incucyte real time imaging platform (Figures SI63 and SI64). The three tested analogs demonstrated much better activity than **1**, consistent with their activity pattern in MDA-MB-231

2D monolayer cultures (Figure 5). **HVS-16** significantly reduced HGF-induced spheroid growth in a dose dependent fashion, with 80% inhibition at 10  $\mu\text{M}$  dose (Figure 5). Interestingly, **39** and **41** were also able to reduce spheroid growth by about 80% at 10  $\mu\text{M}$ , parallel to their antiproliferative activities in MTT assay, despite being 2-fold less active than **HVS-16** in the Z-LYTE™ kinase assay, suggesting other molecular target(s), in addition to c-Met, for their activity. The results of this assay clearly demonstrated the ability of tested analogs to block HGF-driven growth not only in 2D but also in 3D cultures of the human triple negative breast cancer (TNBC), which may in turn suggest a promising in vivo profile for these analogs.

#### **2.2.6. Selective cytotoxic activity evaluation**

The selective cytotoxicity of the new olive secoiridoid bioisosteres was assessed in the MTT assay using the immortalized non-tumorigenic human mammary epithelial cell line MCF10A (Figure 6, Table SI23). The analogs **HVS-16**, **20**, **21**, **24-26**, **28**, **37**, **39**, **41**, **44** and **45** showing the most promising activity in MTT proliferation assay, with  $\text{IC}_{50}$  values  $<10 \mu\text{M}$ , were selected for testing in this assay at different concentrations per each analog and the  $\text{IC}_{50}$  values were determined for proper selectivity assessment (Table SI23). All tested compounds were non-toxic to MCF10A cells, compared to the vehicle-treated control group, at concentrations several-fold higher than their  $\text{IC}_{50}$  values in cell proliferation assay, suggesting their good selectivity towards malignant cells (Figure 6, Table SI23). For instance, **HVS-16**, the most active c-Met phosphorylation inhibitor in the Z-LYTE™ assay, was shown to have no remarkable effect on the viability and growth of non-tumorigenic MCF10A mammary epithelial cells up to 80  $\mu\text{M}$  in culture ( $\text{IC}_{50} = 226.4 \mu\text{M}$ , Table SI23), while it exhibited  $\text{IC}_{50}$  values of 3.8 and 2.5  $\mu\text{M}$  in proliferation and migration assays, respectively, against the MDA-MB-231 cells (Figure 6, Table 2). These results suggested the excellent selectivity of **HVS-16** towards breast

cancerous cells, which renders this analog a potential candidate for the control of invasive breast cancer.

### **2.2.7. Biological characterization of HVS-16**

The enzymatic and cellular results suggested the potential of homovanillyl sinapate (**HVS-16**, Scheme 2) as the most potent synthesized c-Met inhibitory hit (Table 1, Figure 1). **HVS-16** also showed the most potent anticancer activity in different cell-based assays, without discernable effects on the non-tumorigenic human mammary epithelial cells (Figures 3-6). Taken together, **HVS-16** was considered appropriate for further validation of its c-Met inhibitory activity at the molecular level. In order to evaluate its off-target effects, **HVS-16** was tested against the c-Met-independent T-47D human breast cancer cells. This particular cell line represents a completely different breast cancer phenotype, compared to the TNBC phenotype used throughout the study. ER $\alpha$ , one of the most important targets in human breast cancer therapy, is expressed in T-47D cells, whereas the TNBC cells lack the expression of ER $\alpha$  due to epigenetic silencing [41]. On the other hand, c-Met is overexpressed in the TNBC MDA-MB-231 and MDA-MB-468 cells, while it is absent in T-47D cells [42].

#### **2.2.7.1. Effect of HVS-16 on c-Met phosphorylation**

The human TNBC MDA-MB-231 cell line was chosen to assess the effect of **HVS-16** on HGF-induced c-Met phosphorylation using Western blot analysis, to further validate the initial biochemical data. Phospho-c-Met refers to the phosphorylation of the kinase domain at Y1234/1235. Cells were exposed to different doses (1, 5 and 10  $\mu$ M) of **HVS-16** and the expression and phosphorylation levels of c-Met protein in these cell lysates were then determined (Figure 7A). Results demonstrated significant dose-dependent inhibition of HGF-induced c-Met phosphorylation after treatment with **HVS-16** for 72 h, consistent with its

observed cell-free activity and matching the antiproliferative effects (Figure 7). Meanwhile, **HVS-16** treatment did not affect the total c-Met levels at the tested concentrations in vitro (Figure 7A).

#### 2.2.7.2. Evaluation of **HVS-16** off-target effects

The growth inhibitory effect of **HVS-16** on human breast cancer cells with different c-Met status was assessed using MTT assay. The antiproliferative effects of various doses of **HVS-16** on the HGF-mediated growth of the Met-dependent MDA-MB-231, MDA-MB-468, and the Met-independent T-47D breast cancer cell lines, after 72 h culture period are shown in Figure 7B. Treatment with **HVS-16** caused a dose-dependent suppression of HGF-induced proliferation of human breast cancer cells from lines MDA-MB-231 and MDA-MB-468, compared to their vehicle-treated control groups (Figure 7B). Interestingly, larger concentrations of **HVS-16** were required to significantly abolish the cell viability of both cell lines when grown in HGF-free media after 72 h (data not shown). The  $IC_{50}$  values for **HVS-16** treatment in HGF-supplemented media were 3.8 and 6  $\mu$ M in MDA-MB-231 and MDA-MB-468 breast cancer cells, respectively (Figure 7B). However, the  $IC_{50}$  values for **HVS-16** treatment in HGF-free media were  $>40$   $\mu$ M for both cell lines (data not shown). This finding indicated that **HVS-16** treatment is only dependent on the presence of HGF, confirming its proposed molecular mechanism as a direct inhibitor of the HGF/c-Met signaling. Importantly, **HVS-16** lacked activity against the Met-independent T-47D breast cancer cells, being several-fold less active in this cell line compared to the c-Met expressing breast cancer cells ( $IC_{50} = 109.8$   $\mu$ M, Figures 7B and SI65). This result confirmed that the differential sensitivity of the human breast cancer cells to **HVS-16** is linked to its inhibitory effects on c-Met signaling.

The in vitro assays clearly indicated that **HVS-16** significantly and specifically inhibited HGF-dependent cell growth across c-Met-expressing TNBC cell lines. TNBC is characterized by a lack of the expression of the ER, progesterone receptor and HER-2 [43]. It accounts for about 17% of all breast cancers, representing an aggressive clinical behavior and is generally associated with poor prognosis; thus chemotherapy remains the only systemic treatment option available for these patients [43]. Accordingly, there is a need to develop new treatments for this aggressive subtype, which currently lack targeted therapy. The inhibition of mammary cancer cell growth was associated with the ability of **HVS-16** to disrupt c-Met receptor activation in response to HGF in MDA-MB-231 cells. Collectively, these data support the fact that c-Met inhibition can be the primary therapeutic target for the antitumor effects of **HVS-16** in vitro.

### ***2.3. HVS-16 Binding Mode at the c-Met Kinase Domain***

The c-Met's ATP binding site includes: (1) Hinge region: Met1160 and Pro1158. Interaction at this site is highly characteristic for all compounds targeting the ATP binding site in kinase domains; (2) Central hydrophobic region; (3) Two smaller hydrophobic subpockets; and (4) c-Met activation loop (Asp1222-Lys1245) [44]. The central hydrophobic region is usually defined by three important amino acids Lys1110, Val1092, and Met1211. The first hydrophobic subpocket is aligned by Ile1084, Ala1108, and Leu1157 while the second hydrophobic subpocket is defined by Phe1089. There are basically two classes of c-Met inhibitors, ATP competitive and ATP non-competitive inhibitors. About 20 c-Met crystal structures have been disclosed to date, whether in complex with a ligand or not, revealing two distinct binding modes for the ATP competitive inhibitors [2]. The ATP competitive inhibitors are further divided into two classes; class I inhibitors, which are relatively selective and assume an approximate U-shape geometry within the c-Met's ATP-binding site through interactions

with the hinge region's Met1160 and the activation loop residue Tyr1230, while class II inhibitors are less selective, adopting more extended orientation [44]. Overall, a good binding affinity for any c-Met inhibitor hit is hypothesized to be through interactions with at least one of Asp1222, Phe1223, or Tyr1230 at the activation loop and either Pro1158 or Met1160 at the hinge region, along with a good fitting within one or more of the aforementioned hydrophobic regions [2].

A detailed in silico docking analysis was performed to further elucidate the binding mode of **HVS-16** at the c-Met's ATP binding pocket. Docking studies have been carried out separately on different c-Met crystal structures to minimize false positive results due to conformational variations. Four highly resolved c-Met kinase domain crystal structures (PDB codes: 3CE3, 3F82, 3U6I, and 4XYF) at a resolution  $\geq 2$  Å were used to investigate **HVS-16** possible binding modes within the catalytic domain of non-phosphorylated c-Met using Schrödinger software (Figures 8, SI66-67 and SI71-72). In some crystal structures, **HVS-16** assumed a shallow U-shaped binding mode at the c-Met kinase domain with partial wrapping around Met1211, which was the typical conformation of class I c-Met inhibitors [2]. **HVS-16** adopted an extended conformation similar to class II c-Met inhibitors in other crystal structures. Adopting either conformation could be due to different shape and size of the binding cavity existing in various c-Met crystal structures after the originally co-crystallized ligand is removed.

The visualization of the docked pose of **HVS-16** emphasized its complete shape fitting at the ATP binding pocket of c-Met kinase domain (Figures 8E and SI72). The two phenolic hydroxyl groups on the aromatic rings A and B in **HVS-16** were virtually proposed to be the main binding and anchoring pharmacophoric groups at the c-Met kinase domain (Figures 8B, 8C, SI66 and SI67). Detailed examination of **HVS-16** binding pose revealed that the tyrosol's

C-6' phenolic hydroxyl group is either participating in a critical single HB with the backbone of Met1160 or forming a pair of bidentate HB interactions with the backbone of both Met1160 and Pro1158 in the hinge region of the four studied c-Met crystal structures (Figures 8B, 8C, SI66 and SI67). Alternatively, the C-6'-*O*-methyl ether analogs **24** and **26**, which lack free C-6' hydroxyl group, failed to satisfy such critical HB interactions within the hinge region and subsequently showed poor activity in the c-Met biochemical assay (Table 1). This docking result clearly corroborated with the SAR data, which suggested the need for at least one HBD group at the C-6' position. In addition, the aromatic C-7 phenolic hydroxyl group of the sinapic acid moiety formed a strong HB interaction either with the backbone carbonyl oxygen of Glu1127 in crystal structures 3F82 and 3CE3 (Figures 8B and SI67), or with Arg1208 in crystal structure 4XYF (Figure 8C), thus hindering the participation of these residues in catalysis. This HB appeared to impart a substantial portion of the binding affinity, as proven by the activity lack of the previously reported C-7-*O*-methyl ether analogs [19]. The C-7 amino group in analog **33** appeared to maintain this critical HB interaction with the kinase domain, and thus retained the activity in the c-Met biochemical assay (Table 1). The docking results supported the SAR data, which suggested the need for a HBD group at the C-7 position. However, there was an exception related to the lack of this C-7 HB interaction to the phenolic hydroxyl group of **HVS-16** in crystal structure 3U6I (Figure SI66). Instead, the aromatic C-6 methoxy oxygen of sinapic acid was uniquely engaged in a HB interaction with the backbone amide hydrogen of Asp1222 at the activation loop's DFG motif of this crystal structure (Figure SI66). Additionally, the same C-6 methoxy group was buried within a hydrophobic pocket lined by Phe1223 (DFG motif), Met1131, Val1155 and Ala1221 in both crystal structures 3U6I and 4XYF (Figures SI66 and 8C). Despite C-6 methoxy group lacked HB interactions in crystal structures 3F82 and 3CE3, it was able to occupy a hydrophobic pocket defined by Ala1127, Ile1145, Val1155, and

Phe1124 (Figures 8B and SI67). Ile1145 demarcates the back of this pocket, which referred to as the Ile1145 pocket or the C-helix pocket [45]. This pocket has only been reported in a subset of kinases and is present due to the uncharacteristic position of the C-helix, which is further away from the ATP binding site than it is in most kinases [36, 44]. The aromatic C-8 methoxy group of sinapic acid was solvent exposed in all c-Met crystal structures and therefore should not have a significant impact on c-Met inhibition. These interactions underscore the importance of at least one methoxy group in the sinapic acid part of **HVS-16** for binding and subsequent kinase inhibitory capacity, which is consistent with the generated SAR using the cell-free assay. Interestingly, these observations could explain the ability of analog **17** to retain the c-Met inhibitory activity, compared to **HVS-16**, as well as the significant reduction in the potency of **6**, lacking both methoxy groups, versus **4** in the kinase assay (Table 1). In the lipophilic back pocket of the activation loop, the sinapic acid's aromatic ring B is sandwiched between Met1211 and Tyr1230, forming a strong  $\pi$ - $\pi$  stacking interaction with Tyr1230, thus hindering its autophosphorylation necessary for c-Met activation and stabilizing the inhibitory conformation of the activation loop (PDB 4XYF, Figure 8C). The *E*-configuration of the sinapate moiety is presumably essential to maintain the  $\pi$ - $\pi$  stacking interaction of ring B with Tyr1230 as well as the HB interaction of the C-7 phenolic OH and this might be the reason that the *E*-configuration was critical for the c-Met inhibition in the cell-free assay. The terminal 2'-phenethyl part in **HVS-16** occupied a deep hydrophobic pocket defined by Tyr1159, Leu1157, Ala1108, Val1092 and Leu1140 in all c-Met crystal structures (Figure 8). The lower c-Met inhibitory activity of the benzyl derivatives **39** and **41** and the 3'-phenylpropyl analogs **20** and **21** in the cell-free assay, relative to **HVS-16**, suggested that the phenethyl moiety might be optimal for fitting into this hydrophobic pocket.

The key modification that led to improved potency against c-Met involved substitution of the C-5' of **4**'s ring A with a methoxy group in **HVS-16**. This change resulted in 14-fold activity increase in the kinase assay (Table 1). Docking studies further justified this activity enhancement by showing the C-5' methoxy group, despite lacking HB interactions, is buried in the binding pocket and exerting hydrophobic interactions with the side chains of Ile1084, Phe1089, Val1092, and Leu1140 at the c-Met kinase hydrophobic sub-pockets (Figures 8B, 8C, SI66 and SI67). Typically, it resides between Ile1084 and the residue at the tip of the phosphate-binding loop (P-loop), Phe1089. These hydrophobic interactions might explain, at least in part, the significant activity improvement impact of this methoxy group in **HVS-16**, compared to the unsubstituted analog **4**, as well as analogs **13** and **15** with hydroxyl group at this position (Table 1). However, the c-Met inhibitory activity of **HVS-16** is still in the low micromolar level, perhaps because the methoxy group is not sufficiently bulky enough to fill the hydrophobic pocket or lacks the potential to engage in  $\pi$ -electron interactions with the aromatic residues comprising the pocket. The ester moiety appeared not to contribute any binding role, yet it provided the proper molecular size and U-shaped conformation alignment necessary for adequate fitting at the binding pocket (Figures 8, SI66 and SI67). Although the six-atom linker tethered the two aromatic rings A and B did not have direct binding role, it ultimately played a crucial role in properly aligning **HVS-16** binding pharmacophores at the c-Met kinase domain and thus, maintained the critical HB interactions with both the hinge region and the activation loop (Figures 8, SI66 and SI67).

To validate the docking results, the original ligand of each c-Met crystal structure used was docked into its ATP binding pocket by using the same parameters which have been used for docking **HVS-16** (Figures 8D, SI68-70). The bound conformation of the co-crystal ligand was generated with a good root mean square displacement (RMSD) of 0.2 Å, showing the

robustness of the docking protocols. Figure 8D shows the docking model of **HVS-16** in the co-crystal structure of **49** bound to the c-Met kinase (PDB code: 3F82). **HVS-16** almost overlaid the original co-crystallized ligand **49**, demonstrating the same critical interaction with the hinge region's Met1160 [46]. However, **49** engaged in two HB interactions with the backbone amide hydrogen of Asp1222 and the side chain of Lys1110 while **HVS-16** participated in a single HB interaction with Glu1127 (Figure 8D). Despite most parts of the two molecules overlaid perfectly, the terminal 4-fluoro-phenyl ring in **49** extended to occupy a deep hydrophobic pocket defined by Phe1134, Leu1195, and Phe1200 unlike the aromatic C-8 sinapate methoxy group in **HVS-16**, which adopted a different conformation and missed this pocket (Figure 8D). These observations might explain, at least in part, the moderate activity level of **HVS-16** in the c-Met biochemical assay compared to **49** [46]. The docking studies suggested the good fitting of **HVS-16** in the c-Met kinase. The binding mode of **HVS-16** within the catalytic c-Met domain is consistent with the kinase assay data, suggesting the potential of **HVS-16** as a promising c-Met inhibitory hit.

### 3. Conclusion

The present study validated the discovery of **HVS-16** as a novel small-molecule c-Met inhibitory hit inspired by the olive secoiridoid oleocanthal with therapeutic potential for the control of c-Met-dependent breast cancer. The structural simplicity and synthetic feasibility of the olive secoiridoid analogs render them appropriate candidates for future preclinical optimization. The in vitro cellular potency of **HVS-16** in 2D and 3D breast cancer cultures was well-correlated with its cell-free c-Met phosphorylation inhibitory activity coupled with high selectivity to cancerous cells. The novel structure of **HVS-16** provides new opportunities to chemically improve the binding affinity, as shown by docking studies. Collectively, the present

study supported the potential of olive secoiridoids to inspire the discovery of novel c-Met inhibitory entity appropriate for future use to control c-Met-dependent malignancies.

## 4. Materials and Methods

### 4.1. General Experimental Procedures

TLC analysis was carried out on precoated Si gel 60 F<sub>254</sub> 500  $\mu$ m TLC plates (EMD Chemicals), using *n*-hexane-EtOAc (5:5) as a developing system. For column chromatography, Si gel 60 (Natland International Corporation, 230-400  $\mu$ m) and Sephadex LH-20 were used with gradient *n*-hexane-EtOAc as a mobile phase. <sup>1</sup>H and <sup>13</sup>C NMR spectra were recorded in CDCl<sub>3</sub>, using tetramethylsilane (TMS) as an internal standard, on a JEOL Eclipse-ECS NMR spectrometer operating at 400 MHz for <sup>1</sup>H NMR and 100 MHz for <sup>13</sup>C NMR. HRESIMS experiments were conducted using a JEOL JMS-T100 LP AccuTOF LC-Plus, equipped with an ESI source (JEOL Co. Ltd., Tokyo, Japan). ESI-MS detection was set using negative ion mode as described previously [38]. Results were obtained using Mass Center software, MS-56010MP.

### 4.2. Chemicals, Reagents, and Antibodies

All chemicals were purchased from Sigma-Aldrich (St. Louis, MO), unless otherwise stated. (-)-Oleocanthal (**1**) and ligstroside (**2**) were isolated from EVOO as previously described [19]. 4-Hydroxy-3,5-dimethoxybenzyl alcohol, 4-(3-hydroxypropyl)-2-methoxyphenol, and (6-amino pyridin-3-yl)methanol were purchased from VWR (Suwanee, GA). All antibodies were purchased from Cell Signaling Technologies (Beverly, MA) and used at a dilution of 1:1,000. Human recombinant HGF growth factor was acquired from PeproTech Inc. (Rocky Hill, NJ).

### 4.3. Chemical Synthesis

#### 4.3.1. Preparation of analogs 5-9 and 13-47 by chemoselective Mitsunobu esterification

Triphenylphosphine (TPP) (280 mg, 1.07 mmol) was added in portions to a freshly prepared solution of the designated alcohol (1.0 mmol) and the specified phenolic acid (1.0 mmol equivalent) in anhydrous THF (3.5 mL) at 0 °C. Diisopropylazodicarboxylate (DIAD) (208  $\mu$ L, 1.0 mmol) was then added dropwise to the mixture. The reaction mixture was stirred at 0 °C for 30 minutes. The mixture was then warmed and stirring was continued for 48 h at rt [19]. Reactions were monitored till completion by TLC. The reaction mixture was then worked up by removal of the solvent under reduced pressure, saturated solution of NaHCO<sub>3</sub> (10 mL) was added, and then the mixture was extracted with EtOAc (3 x 20 mL). The combined organic layers were washed with brine, dried over anhydrous Na<sub>2</sub>SO<sub>4</sub>, filtered, and the filtrate was evaporated under reduced pressure to dryness. The crude product was collected and purified by column chromatography (CC) on Sephadex LH-20 using isocratic CH<sub>2</sub>Cl<sub>2</sub> followed by chromatography on Si gel 60 using *n*-hexane-EtOAc system, gradient elution, to afford **5-9** and **13-47** (Supplementary Information).

#### **4.3.2. Preparation of analog 10**

Sinapic acid (224.2 mg, 1.0 mmol) and triethylamine (TEA) (1.5 equivalents) were mixed in DMF (3.5 mL) and then tyramine (137.2 mg, 1.0 mmol) was added to the mixture. BOP (1.5 mL) in anhydrous CH<sub>2</sub>Cl<sub>2</sub> was then added and the resulting mixture was stirred for 30 min in ice bath. The reaction mixture was kept stirring at rt for 24 h. Once the reaction completed, evidenced by TLC monitoring, the crude product was purified by CC on Sephadex LH-20 using gradient CH<sub>2</sub>Cl<sub>2</sub>-MeOH system to afford **10** (Supplementary Information).

#### **4.3.3. Preparation of analog 11**

A mixture of sinapaldehyde (208.2, 1.0 mmol) and tyramine (137.2 mg, 1.0 mmol) in 10 mL MeOH was stirred at rt for 1 h to give a red precipitate. The precipitate was filtered and washed twice with MeOH to afford **11** (Supplementary Information).

#### **4.3.4. Preparation of analog 12**

Sinapic acid (44.8 mg, 0.2 mmol) was mixed in 15 mL CH<sub>2</sub>Cl<sub>2</sub> with 4-hydroxybenzamidinium oxime (30.4 mg, 0.2 mmol) and EDCI (93.1 mg, 0.6 mmol) was then added as a coupling reagent. The mixture was stirred under reflux for 24 h. The mixture was cooled to rt, diluted with H<sub>2</sub>O (10 mL) and extracted with EtOAc (3 x 20 mL). The organic phases were combined, dried over anhydrous Na<sub>2</sub>SO<sub>4</sub> and then concentrated under vacuum. The residue was subjected to Si gel CC using gradient *n*-hexane-EtOAc to afford **12** (Supplementary Information).

#### **4.4. In Vitro Assays**

##### **4.4.1. Biochemical kinase assay**

The Z-LYTE™ Kinase Assay-Tyr6 Peptide kit (Life Sciences) was used to assess the ability of synthesized analogs to inhibit the catalytic activity of c-Met kinase (Product# PV3143). Briefly, 20 µL/well reactions were set up in 96-well plates containing kinase buffer, 200 µM ATP, 4 µM Z-LYTE™ Tyr6 Peptide substrate, 2500 ng mL<sup>-1</sup> c-Met kinase and tested compound as an inhibitor. After 1 h of incubation at rt, 10 µL development solution containing site-specific protease was added to each well. Incubation was continued for 1 h. The reaction was then stopped, and the fluorescent signal ratio of 445 nm (coumarin)/520 nm (fluorescein) was determined on a plate reader (BioTek FLx800™), which reflects the peptide substrate cleavage status and/or the kinase inhibitory activity in the reaction.

##### **4.4.2. Cell lines and culture conditions**

The human breast cancer cell lines and the non-tumorigenic human mammary epithelial MCF10A cells were purchased from the ATCC (Manassas, VA). All cancer cell lines were maintained in RPMI-1640 (GIBCO-Invitrogen, NY) supplemented with 10% fetal bovine serum (FBS) (Gemini Bio-Products), 100 U/mL penicillin G, 100 µg/mL streptomycin and 2 mmol/L glutamine. The MCF10A cells were cultured in DMEM/F12 supplemented with 5% horse serum, 0.5 µg/mL hydrocortisone, 20 ng/mL EGF, 100 U/mL penicillin G, 100 ng/mL cholera toxin, 100 µg/mL streptomycin, and 10 µg/mL insulin. All cells were maintained at 37°C in a humidified incubator under 5% CO<sub>2</sub>. A stock solution was prepared by dissolving each tested analog in sterilized DMSO at a concentration of 10 mM for all assays. Working solutions at their final concentrations for each assay were prepared in appropriate culture medium immediately prior to use. The vehicle control was prepared by adding the maximum volume of DMSO, used in preparing test compounds, to the appropriate media type such that the final DMSO concentration was maintained as the same in all treatment groups within a given experiment and never exceeded 0.1%. **1** was used as a positive control at 10 µM based on earlier studies [19, 23].

#### ***4.4.3. Measurement of viable cell number***

Viable cell count was determined using the MTT colorimetric assay. The optical density of each sample was measured at 570 nm on a Synergy 2 microplate reader (BioTek, VT, USA). The number of cells per well was calculated against a standard curve prepared at the start of each experiment by plating various concentrations of cells (1,000-60,000 cells per well), as determined using a hemocytometer [23].

#### ***4.4.4. MTT proliferation assay***

MDA-MB-231, MDA-MB-468, and T-47D cells, in exponential growth, were seeded at a density of  $1 \times 10^4$  cells per well (6 wells/group) in 96-well culture plates and maintained in RPMI-1640 media supplemented with 10% FBS and allowed to adhere overnight at 37°C under 5% CO<sub>2</sub> in a humidified incubator. The next day, cells were washed with phosphate buffer saline (PBS), divided into different treatment groups and then fed serum-free defined RPMI-1640 media containing HGF (40 ng/mL as a mitogen which induced maximum growth in the three cell lines after 72 h) or no HGF (0.5% FBS was added to the media to maintain the viability of the cells throughout the experiment) and experimental treatments (containing designated concentrations of the tested compounds) or vehicle-treated control media and incubation resumed at 37°C under 5% CO<sub>2</sub> for 72 h. Cells in all groups were fed fresh treatment media every other day during the 72 h treatment period. Control and treatment media were then removed, replaced with fresh media, and 50 µL fresh MTT solution (1 mg mL<sup>-1</sup>) was added to each well and plates were re-incubated for 4 h at 37 °C. The color reaction was stopped by removing the media and adding 100 µL DMSO in each well to dissolve the formed formazan crystals. Incubation at 37°C was resumed for up to 20 minutes to ensure complete dissolution of crystals. Absorbance was determined at  $\lambda$  570 nm using an ELISA plate microreader (BioTek, VT, USA) [47]. The % cell survival was calculated as follows: % cell survival = (Cell No.<sub>treatment</sub>/Cell No.<sub>DMSO</sub>) x 100.

The cytotoxic effect of synthesized analogs was evaluated against the non-tumorigenic human mammary epithelial cell line MCF10A. Cells in exponential growth were seeded at a density of  $1 \times 10^4$  cells per well into 96-well plates, maintained in DMEM/F12 media containing 5% horse serum, and allowed to attach overnight under 5% CO<sub>2</sub>. The next day, cells were washed with PBS, divided into different treatment groups and then treated with appropriate control or tested compounds in fresh serum-free defined media containing 40 ng/mL HGF, each

in triplicate, and re-incubated for 24 h. Viable cell number was determined using the MTT assay.

#### 4.4.5. Wound healing assay (WHA)

MDA-MB-231 cells were plated in sterile 24-well plates and allowed to form a confluent monolayer per well overnight. Wounds were then inflicted in each cell monolayer using a sterile 200  $\mu$ L pipette tip. The media were removed and cells were washed twice with PBS and once with fresh RPMI medium to remove cell debris. Test compound concentrations were prepared in fresh serum-free defined media, containing 40 ng/mL HGF as a mitogen, and were added to wells in triplicate. Cells were incubated for 24 h after which, the medium was removed and cells were washed, fixed, and stained using Giemsa stain. Wound healing was visualized at 0 and 24 h by a Nikon ECLIPSE TE200-U microscope and digital images were captured using Nikon NIS Elements software (Nikon Instruments Inc., Melville, NY) (Figure 3B). The distance traveled by the cells was determined by measuring the wound width after 24 h. Percentages cell migration were calculated using the following formula:

$$\text{Percent cell migration} = \frac{[T_0 - T_t - T_{\text{dms0}}]}{T_0 - T_{\text{dms0}}} \times 100$$

Where,  $T_0$  is wound thickness at zero time,  $T_{\text{dms0}}$  is wound thickness in DMSO-treated control wells and  $T_t$  is wound thickness in treated wells.

#### 4.4.6. Cultrex<sup>®</sup> BME cell invasion assay

The Cultrex<sup>®</sup> BME cell invasion assay (Trevigen, Inc., Gaithersburg, MD) was conducted according to the vendor's protocol [48]. The top invasion chamber inserts were coated with 50  $\mu$ L/well of 1X BME solution and incubated overnight at 37°C under 5% CO<sub>2</sub>. The coating solution was then aspirated off and 50,000/50  $\mu$ L of MDA-MB-231 cells suspended in fresh RPMI-1640 medium were then seeded to each well in the top chamber. Tested

compounds were prepared, in serum-free medium supplemented with 40 ng/mL HGF, at 6X the desired concentrations and 10  $\mu$ L of each tested concentration was added in triplicate to the wells of the top chamber to achieve the final test concentrations (1, 5, 10 and 20  $\mu$ M). About 150  $\mu$ L of RPMI-1640 medium, containing 10% FBS and penicillin/streptomycin as well as fibronectin (1  $\mu$ L/mL) and *N*-formyl-Met-Leu-Phe (10 nM) as chemoattractants, was then added to each well in the lower chamber. Plates were gathered and re-incubated at 37°C under 5% CO<sub>2</sub> for 24 h after which the both chambers were carefully aspirated and washed with 100  $\mu$ L/well washing buffer supplemented with the kit. About 100  $\mu$ L of cell dissociation/calcein-AM solution was added to each well in the bottom chamber and the plate was incubated at 37°C under 5% CO<sub>2</sub> for 1 h. The cells internalize calcein-AM, and the intracellular esterases cleave the acetomethyl ester (AM) moiety to generate free calcein. Fluorescence of samples was measured at  $\lambda_{\text{excitation}}$  485 nm and  $\lambda_{\text{emission}}$  528 nm using an ELISA plate reader (BioTek, VT, USA). Relative fluorescence units (RFU) were used to calculate the number of cells invaded through the BME coat using a standard curve prepared by plating various numbers of cells prior to the experiment. Mean percent invasion of different treatments was calculated in relative to the DMSO-treated control wells.

#### **4.4.7. 3D-Spheroid disaggregation assay**

MDA-MB-231 cells were collected after trypsinization and resuspended in phenol-red free DMEM supplemented with 10% FBS. Cells were then labeled with CellTracker Red (Life Technologies) for 5 min. After labeling, cells were washed with PBS and seeded into 96-well Corning 7007 ULA round bottom low cell attachment plates at a density of 1,000 cells/well suspended in 100  $\mu$ L phenol-red free media, supplemented with 10% FBS and 5% Matrigel. This protocol resulted in the formation of a single spheroid in the center of each well of

identical size, after 24 h. Spheroids were supplemented either with DMSO as vehicle control or with designated concentrations of **HVS-16**, **39** and **41**. Spheroids were incubated at 37°C and 5% CO<sub>2</sub> in IncuCyte ZOOM Real Time Imaging System (Essen Bioscience) and images were automatically acquired every 4 h for a period of 72 h post-treatment. The software associated with the IncuCyte was designed to identify the red object in each well and calculate the average area of each spheroid. The data were expressed as fold increase in spheroids size at the end of the experiment using the average red object area in each well. The assay was repeated twice and performed with 8 spheroids per treatment group.

#### **4.4.8. Western blot analysis**

MDA-MB-231 human breast cancer cells were initially plated and prepared for Western blot analysis according to the method previously described [23]. The whole-cell extracts were prepared in RIPA buffer (Qiagen Sciences Inc., Valencia, CA). Protein concentration was determined by the BCA assay (Bio-Rad Laboratories, Hercules, CA) according to the manufacturer's instructions. Equivalent amounts of protein were electrophoresed on SDS-polyacrylamide gels. The gels were then electroblotted onto PVDF membranes. These PVDF membranes were then blocked with 2% BSA in 10 mM Tris-HCl containing 50 mM NaCl and 0.1% Tween 20, pH 7.4 (TBST) and then, probed with the indicated specific primary antibodies overnight at 4°C. Membranes were then washed extensively with TBST and incubated with respective horseradish peroxidase-conjugated anti-rabbit or anti-mouse secondary anti-bodies in 2% BSA in TBST for 1 h at rt followed by rinsing with TBST for 5 times. Blots were then visualized using an enhanced chemiluminescence according to the manufacturer's instructions (Pierce, Rockford, IL, USA). Images of protein bands from all treatment groups were acquired using Kodak Gel Logic 1500 Imaging System (Carestream Health Inc, CT, USA). The

visualization of  $\beta$ -tubulin was used to ensure equal sample loading in each lane. The experiment was repeated three times and a representative Western blot image is shown in Figure 7A.

#### **4.5. Molecular Modeling**

The in silico experiments were carried out using Schrödinger molecular modeling software package installed on an iMac 27-inch Z0PG workstation with a 3.5 GHz Quad-core Intel Core i7, Turbo Boost up to 3.9 GHz, processor and 16 GB RAM (Apple, Cupertino, CA, USA).

##### **4.5.1. Protein structure preparation**

Four X-ray crystal structures of the c-Met tyrosine kinase domain; (PDB codes: 3CE3 [49], 3F82 [46], 4XYF [50] and 3U6I [51]) were retrieved from the PDB ([www.rcsb.org](http://www.rcsb.org)). The Protein Preparation Wizard was implemented to prepare the kinase domain of each protein. The protein was reprocessed by assigning bond orders, adding hydrogens, creating disulfide bonds and optimizing H-bonding networks using PROPKA (Jensen Research Group, Denmark) [52]. Finally, energy minimization with RMSD value of  $0.3^{\circ}\text{A}$  was applied using an Optimized Potentials for Liquid Simulation (OPLS\_2005, Schrödinger, New York, USA) force field.

##### **4.5.2. Ligand structure preparation**

The chemical structure of **HVS-16** was sketched on the Maestro 9.3 panel interface (Maestro, version 9.3, 2012, Schrödinger, USA). The Lig Prep 2.3 module (Lig Prep, version 2.3, 2012, Schrödinger, USA) was implemented to generate the 3D structure and to search for different conformers. The OPLS (OPLS\_2005, Schrödinger, USA) force field was applied to geometrically optimize the ligand structure and to compute partial atomic charges. Finally, 32 poses per ligand were generated with different steric features for subsequent docking studies.

### 4.5.3. Molecular docking

The prepared X-ray crystal structures of c-Met were used to generate receptor energy grids applying the default value of the protein atomic scale (1.0°A) within the cubic box centered on the co-crystallized ligand of each crystal structure. **HVS-16** was then docked using the Glide 5.8 module (Glide, version 5.8, 2012, Schrödinger, USA) in extra-precision (XP) mode [53].

### 4.6. Statistics

The results are presented as the means  $\pm$  SEM of at least three independent experiments. Differences among various treatment groups were determined by ANOVA followed by Dunnett's test using PASW statistics<sup>®</sup> version 18 (Quarry Bay, Hong Kong). A difference of  $p < 0.05$  was considered statistically significant compared to the vehicle-treated control group. The IC<sub>50</sub> values were determined using a non-linear regression curve fitting analysis using GraphPad Prism software version 6 (La Jolla, CA, USA).

## Acknowledgments

Research reported in this publication was supported by the National Cancer Institute of the National Institutes of Health under Award Number R15CA167475. The content is solely the responsibility of the authors and does not necessarily represent the official views of the National Institutes of Health. The funders had no role in study design, data collection and analysis, decision to publish, or preparation of the manuscript.

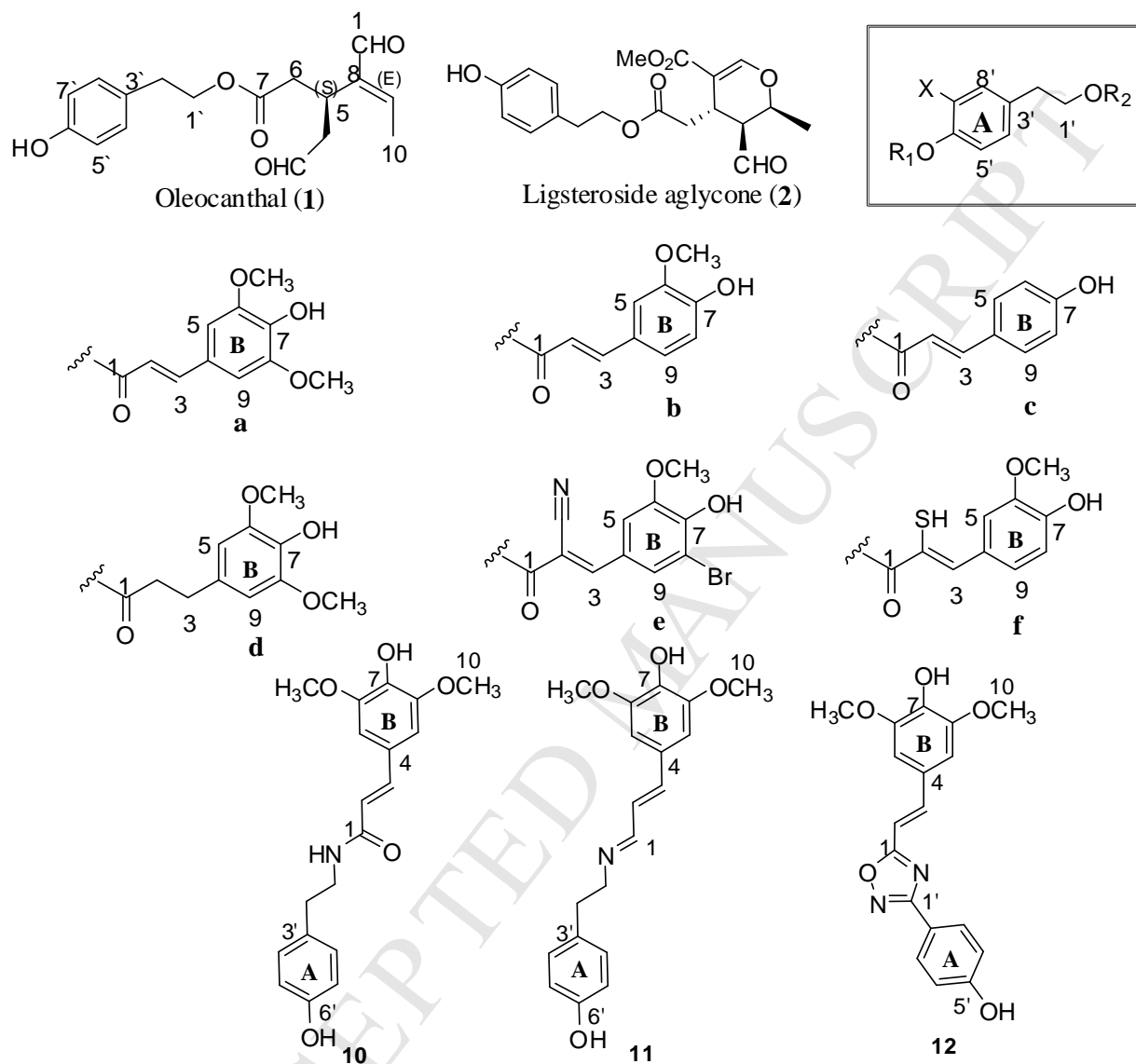
## References

- [1] J.R. Sierra, M.-S. Tsao. *Ther Adv Med Oncol.* 3 (2011) S21-S35.
- [2] E. Gherardi, W. Birchmeier, C. Birchmeier, G. Vande Woude. *Nat Rev Cancer.* 12 (2012) 89-103.
- [3] L. Trusolino, A. Bertotti, P.M. Comoglio. *Nat Rev Mol Cell Biol.* 11 (2010) 834-848.

- [4] L. Schmidt, F.-M. Duh, F. Chen, T. Kishida, G. Glenn, B. Zbar. *Nat Genet.* 16 (1997) 68-73.
- [5] P.C. Ma, S. Jagadeesh, R. Jagadeeswaran, E.A. Fox, J. Christensen, G. Maulik, K. Naoki, E. Schaefer, A. Lader, W. Richards, D. Sugarbaker, M. Meyerson, R. Salgia. *Cancer Res.* 64 (2004) 430-431.
- [6] M.F. Di Renzo, M. Olivero, T. Martone, A. Maffe, P. Maggiora, A.D. Stefani, G. Valente, S. Giordano, G. Cortesina, P.M. Comoglio. *Oncogene.* 19 (2000) 1547-1555.
- [7] C. Ho-Yen, J. Jones, S. Kermorgant. *Breast Cancer Res.* 17 (2015) 52-62.
- [8] A. Varkaris, P.G. Corn, S. Gaur, F. Dayyani, C.J. Logothetis, G.E. Gallick. *Expert Opin Investig Drugs.* 20 (2011) 1677-1684.
- [9] J.H. Lee, S.U. Han, H. Cho, B. Jennings, B. Gerrard, M. Dean, L. Schmidt, B. Zbar, G.F. Vande Woude. *Oncogene.* 19 (2000) 4947-4953.
- [10] Jane D. Holland, B. Györffy, R. Vogel, K. Eckert, G. Valenti, L. Fang, P. Lohneis, S. Elez Kurtaj, U. Ziebold, W. Birchmeier. *Cell Rep.* 5 (2013) 1214-1227.
- [11] U. Drebber, S.E. Baldus, B. Nolden, G. Grass, E. Bollschweiler, H.P. Dienes, A.H. Holscher, S.P. Monig. *Oncol Rep.* 19 (2008) 1477-1483.
- [12] T.R. Wilson, J. Fridlyand, Y. Yan, E. Penuel, L. Burton, E. Chan, J. Peng, E. Lin, Y. Wang, J. Sosman, A. Ribas, J. Li, J. Moffat, D.P. Sutherland, H. Koeppen, M. Merchant, R. Neve, J. Settleman. *Nature.* 487 (2012) 505-509.
- [13] A.B. Turke, K. Zejnullahu, Y.-L. Wu, Y. Song, D. Dias-Santagata, E. Lifshits, L. Toschi, J.A. Engelman, P.A. Jänne. *Cancer Cell.* 17 (2010) 77-88.
- [14] D. Dorsch, O. Schadt, F. Stieber, M. Meyring, U. Gradler, F. Bladt, M. Friese-Hamim, C. Knuhl, U. Pehl, A. Blaukat. *Bioorg Med Chem Lett.* 25 (2015) 1597-1602.
- [15] J.J. Cui. *J Med Chem.* 57 (2013) 4427-4453.
- [16] R. Nuwer. *Sci Am.* 308 (2013) 22.
- [17] A. Giacosa, R. Barale, L. Bavaresco, P. Gatenby, V. Gerbi, J. Janssens, B. Johnston, K. Kas, C. La Vecchia, P. Mainguet, P. Morazzoni, E. Negri, C. Pelucchi, M. Pezzotti, M. Rondanelli. *Eur J Cancer Prev.* 22 (2013) 90-95.
- [18] A.H. Abuznait, H. Qosa, B.A. Busnena, K.A. El Sayed, A. Kaddoumi. *ACS Chem Neurosci.* 4 (2013) 973-982.
- [19] B.A. Busnena, A.I. Foudah, T. Melancon, K.A. El Sayed. *Bioorg Med Chem.* 21 (2013) 2117-2127.
- [20] A. Elnagar, P. Sylvester, K. El Sayed. *Planta Med.* 77 (2011) 1013-1019.
- [21] L. Parkinson, R. Keast. *Int J Mol Sci.* 15 (2014) 12323-12334.
- [22] H. Qosa, Y.S. Batarseh, M.M. Mohyeldin, K.A. El Sayed, J.N. Keller, A. Kaddoumi. *ACS Chem Neurosci.* 6 (2015) 1849-1859.
- [23] M.R. Akl, N.M. Ayoub, M.M. Mohyeldin, B.A. Busnena, A.I. Foudah, Y.-Y. Liu, K.A. El Sayed. *PLoS One.* 9 (2014) e97622.
- [24] L. Margarucci, M.C. Monti, C. Cassiano, M. Mozzicafreddo, M. Angeletti, R. Riccio, A. Tosco, A. Casapullo. *Chem Commun.* 49 (2013) 5844-5846.
- [25] M. Kikuchi, N. Mano, Y. Uehara, K. Machida, M. Kikuchi. *J Nat Med.* 65 (2011) 237-240.
- [26] H. Nakata, Y. Sashida, H. Shimomura. *Chem Pharm Bull.* 30 (1982) 4554-4556.
- [27] Z. Li, Z. Chao, K. Chen. *Shanghai Yike Daxue Xuebao.* 15 (1988) 68-70.
- [28] Y.-T. Lee, M.-J. Don, P.-S. Hung, Y.-C. Shen, Y.-S. Lo, K.-W. Chang, C.-F. Chen, L.-K. Ho. *Cancer Lett.* 223 (2005) 19-25.
- [29] M.H. Chaves, N.F. Roque. *Phytochemistry.* 46 (1997) 879-881.

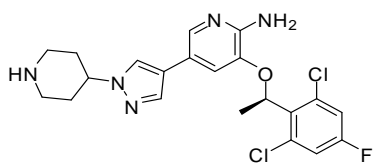
- [30] J.-J. Chen, H.-C. Hung, P.-J. Sung, I.-S. Chen, W.-L. Kuo. *Phytochemistry*. 72 (2011) 523-532.
- [31] H. Tanaka, S. Yatsunami, T. Yasuda, M. Sato, E. Sakai, C. Xiao, H. Murata, J. Murata. *J Nat Med*. 63 (2009) 331-334.
- [32] S. Okombi, D. Rival, A. Boumendjel, A.-M. Mariotte, E.J.L. Perrier. US20070183996 A1 (2007) 66pp.
- [33] K. Izumiyama, T. Sasaya. *Mokuzai Gakkaishi*. 18 (1972) 579-580.
- [34] M.A. Metwally, R.M. King, H. Robinson. *Phytochemistry*. 24 (1985) 182-183.
- [35] C. Chen, C. Wu, X. Lu, Z. Yan, J. Gao, H. Zhao, S. Li. *Evid Based Complement Alternat Med*. 2013 (2013) 639083.
- [36] S.F. Bellon, P. Kaplan-Lefko, Y. Yang, Y. Zhang, J. Moriguchi, K. Rex, C.W. Johnson, P.E. Rose, A.M. Long, A.B. O'Connor, Y. Gu, A. Coxon, T.S. Kim, A. Tasker, T.L. Burgess, I. Dussault. *J Biol Chem*. 283 (2008) 2675-2683.
- [37] J.J. Cui, M. Tran-Dube, H. Shen, M. Nambu, P.P. Kung, M. Pairish, L. Jia, J. Meng, L. Funk, I. Botrous, M. McTigue, N. Grodsky, K. Ryan, E. Padrique, G. Alton, S. Timofeevski, S. Yamazaki, Q. Li, H. Zou, J. Christensen, B. Mroczkowski, S. Bender, R.S. Kania, M.P. Edwards. *J Med Chem*. 54 (2011) 6342-6363.
- [38] A.A. Sallam, M.M. Mohyeldin, A.I. Foudah, M.R. Akl, S. Nazzal, S.A. Meyer, Y.-Y. Liu, K.A. El Sayed. *Org Biomol Chem*. 12 (2014) 5295-5303.
- [39] L. Shaw. *Cell Migration*. 294 (2005) 97-105.
- [40] F. Hirschhaeuser, H. Menne, C. Dittfeld, J. West, W. Mueller-Klieser, L.A. Kunz-Schughart. *J Biotechnol*. 148 (2010) 3-15.
- [41] D. Holliday, V. Speirs. *Breast Cancer Res*. 13 (2011) 215-221.
- [42] L. Beviglia, K. Matsumoto, C.S. Lin, B.L. Ziober, R.H. Kramer. *Int J Cancer*. 74 (1997) 301-309.
- [43] M. Arnedos, C. Bihan, S. Delaloue, F. Andre. *Ther Adv Med Oncol*. 4 (2012) 195-210.
- [44] N. Schiering, S. Knapp, M. Marconi, M.M. Flocco, J. Cui, R. Perego, L. Rusconi, C. Cristiani. *Proc Natl Acad Sci U S A*. 100 (2003) 12654-12659.
- [45] N.D. D'Angelo, S.F. Bellon, S.K. Booker, Y. Cheng, A. Coxon, C. Dominguez, I. Fellows, D. Hoffman, R. Hungate, P. Kaplan-Lefko, M.R. Lee, C. Li, L. Liu, E. Rainbeau, P.J. Reider, K. Rex, A. Siegmund, T.L. Burgess, I. Dussault, T.S. Kim. *J Med Chem*. 51 (2008) 5766-5779.
- [46] G.M. Schroeder, Y. An, Z.W. Cai, X.T. Chen, C. Clark, L.A. Cornelius, J. Dai, J. Gullo-Brown, Y. Zhang, J. Fargnoli, R.M. Borzilleri. *J Med Chem*. 52 (2009) 1251-1254.
- [47] Trevigen. Inc, TACS MTT assays: cell proliferation and viability assays. (2003) 2-7.
- [48] Cultrex® BME cell invasion assay protocol. [www.trevigen.com](http://www.trevigen.com) (accessed 12.01.13).
- [49] K.S. Kim, L. Zhang, R. Schmidt, Z.W. Cai, D. Wei, D.K. Williams, L.J. Lombardo, V. Manne, J.T. Hunt, J. Fargnoli, R.M. Borzilleri. *J Med Chem*. 51 (2008) 5330-5341.
- [50] E.A. Peterson, Y. Teffera, B.K. Albrecht, D. Bauer, S.F. Bellon, A. Boezio, C. Boezio, M.A. Broome, D. Choquette, K.W. Copeland, I. Dussault, R. Lewis, M.H. Lin, J. Lohman, J. Liu, M. Potashman, K. Rex, R. Shimanovich, D.A. Whittington, K.R. Vaida, J.C. Harmange. *J Med Chem*. 58 (2015) 2417-2430.
- [51] M.H. Norman, L. Liu, M. Lee, N. Xi, I. Fellows, N.D. D'Angelo, C. Dominguez, K. Rex, S.F. Bellon, T.S. Kim, I. Dussault. *J Med Chem*. 55 (2012) 1858-1867.
- [52] M.H.M. Olsson, C.R. Søndergaard, M. Rostkowski, J.H. Jensen. *J Chem Theory Comput*. 7 (2011) 525-537.

[53] R.A. Friesner, R.B. Murphy, M.P. Repasky, L.L. Frye, J.R. Greenwood, T.A. Halgren, P.C. Sanschagrin, D.T. Mainz. *J Med Chem.* 49 (2006) 6177-6196.

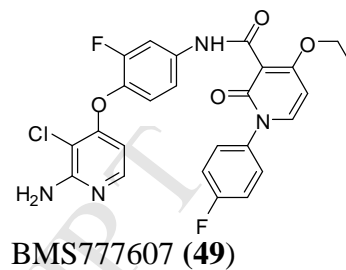
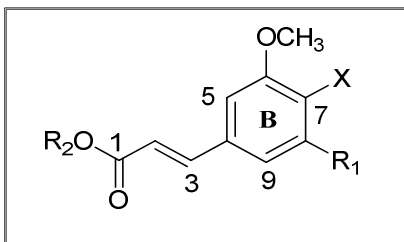


Compound	3	4	5	6	7	8	9	13	14	15
R <sub>1</sub>	H	H	H	H	H	H	H	H	H	H
R <sub>2</sub>	H	a	b	c	d	e	f	a	c	b
X	H	H	H	H	H	H	H	OH	OH	OH

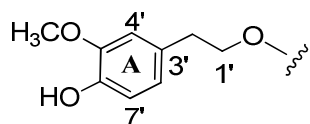
Scheme 1.



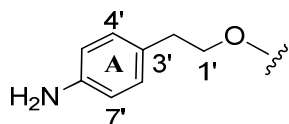
Crizotinib (48)



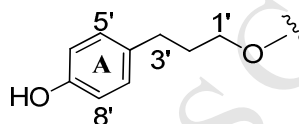
BMS777607 (49)



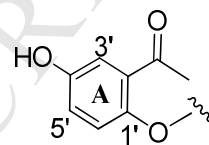
g



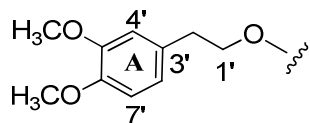
h



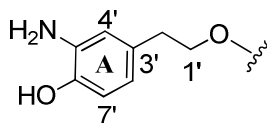
i



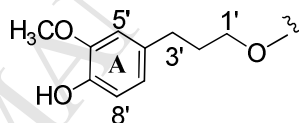
j



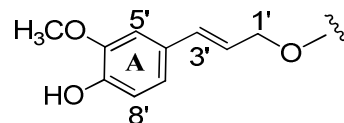
k



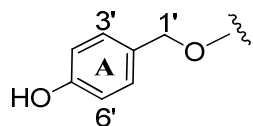
l



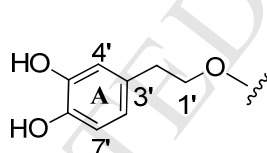
m



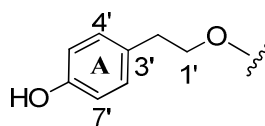
n



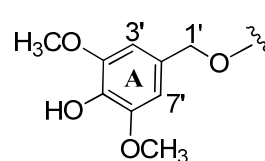
o



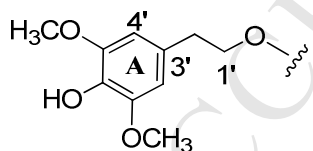
p



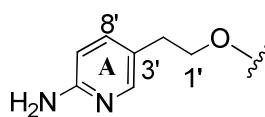
q



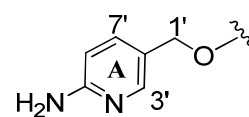
r



s



t



u

Compound	R <sub>1</sub>	R <sub>2</sub>	X	E/Z
16	OCH <sub>3</sub>	g	OH	<i>E</i>
17	H	g	OH	<i>E</i>
18	H	h	OH	<i>E</i>
19	OCH <sub>3</sub>	h	OH	<i>E</i>
20	H	i	OH	<i>E</i>
21	OCH <sub>3</sub>	i	OH	<i>E</i>
22	H	j	OH	<i>E</i>
23	OCH <sub>3</sub>	j	OH	<i>E</i>
24	H	k	OH	<i>E</i>
25	H	k	OH	<i>Z</i>
26	OCH <sub>3</sub>	k	OH	<i>E</i>
27	OCH <sub>3</sub>	k	OH	<i>Z</i>
28	OCH <sub>3</sub>	l	OH	<i>E</i>
29	H	m	OH	<i>E</i>
30	OCH <sub>3</sub>	m	OH	<i>E</i>
31	OCH <sub>3</sub>	n	OH	<i>E</i>
32	OCH <sub>3</sub>	o	OH	<i>E</i>
33	H	g	NH <sub>2</sub>	<i>E</i>
34	H	g	NH <sub>2</sub>	<i>Z</i>
35	H	i	NH <sub>2</sub>	<i>E</i>
36	H	i	NH <sub>2</sub>	<i>Z</i>
37	H	p	NH <sub>2</sub>	<i>E</i>
38	H	q	NH <sub>2</sub>	<i>E</i>
39	H	r	OH	<i>E</i>
40	H	n	OH	<i>E</i>
41	OCH <sub>3</sub>	r	OH	<i>E</i>
42	OCH <sub>3</sub>	s	OH	<i>E</i>
43	H	s	OH	<i>E</i>
44	OCH <sub>3</sub>	t	OH	<i>E</i>
45	H	t	OH	<i>E</i>
46	H	u	OH	<i>E</i>
47	OCH <sub>3</sub>	u	OH	<i>E</i>

Scheme 2.

### Scheme Legends

**Scheme 1.** Chemical structures of natural olive secoiridoids and semisynthetic analogs **1-15**.

**Scheme 2.** Chemical structures of analogs **16-47**, crizotinib (**48**), and BMS-777607 (**49**).

### Figure Legends

**Figure 1.** c-Met phosphorylation inhibition by various doses of the most active analogs **16**, **17**, **33**, **39**, and **41-45** using Z'-LYTE assay kit. Error bars indicate the SEM of N=3/dose; Compounds **1** and **4** were used as positive controls at 5 and 10  $\mu$ M, respectively [19, 20].

**Figure 2.** Effect of various doses of analogs **21**, **39**, and **41** on the viability of the highly metastatic MDA-MB-231 breast cancer cells, upon HGF stimulation, compared to DMSO as a vehicle control. Viable cell count was determined using MTT assay. Error bars indicate the SEM of N=3/dose. **1** was used as a positive control at 10  $\mu$ M [23].

**Figure 3.** (A) Effect of various doses of analogs **HVS-16**, **44** and **45** on HGF-induced MDA-MB-231 breast cancer cell migration in WHA, compared to DMSO as a vehicle control. Error bars indicate the SEM of N=3/dose. Compounds **1** and **4** were used as positive controls at 10 and 20  $\mu$ M, respectively [19]. (B) Antimigratory activity of **HVS-16** against MDA-MB-231 cells in WHA at a single concentration (5  $\mu$ M), compared to DMSO as a vehicle control.

**Figure 4.** Effect of various doses of analogs **HVS-16**, **21** and **39** on HGF-induced MDA-MB-231 breast cancer cell invasion in Cultrex<sup>®</sup> BME assay, compared to DMSO as a vehicle control. Error bars indicate the SEM of N=3/dose. **1** and **4** were used as positive controls at 20  $\mu$ M [19].

**Figure 5.** Effect of analogs **HVS-16**, **39** and **41** on the growth of MDA-MB-231 cells cultured as 3D spheroids, upon HGF stimulation, compared to DMSO as a vehicle control. Spheroids were grown at 37°C and 5% CO<sub>2</sub> for 72 h in IncuCyte ZOOM. Images were acquired every 4 h and the data were expressed as fold increase in spheroids size at the end of the treatment using the average red object area in each well as determined by the IncuCyte software analysis. Error bars indicate the SEM of N=3/dose. **1** was used as a positive control at 20  $\mu$ M.

**Figure 6.** Cytotoxic activities of analogs **16**, **20**, **21**, **24-26**, **28**, **37**, **39**, **41**, **44** and **45** against the non-tumorigenic human mammary epithelial cell line MCF10A, compared to DMSO as a vehicle control. Error bars indicate the SEM of N=3/dose.

**Figure 7.** (A) Effect of **HVS-16** treatment on HGF-induced c-Met activation in human breast cancer cells using Western blot analysis. **HVS-16** treatment caused a dose-dependent inhibition of HGF-induced c-Met phosphorylation in MDA-MB-231 cells without any effect on total c-Met levels after treatment for 72 h, compared to vehicle-treated control group. The visualization of  $\beta$ -tubulin was used as a loading control. (B) Effect of **HVS-16** treatment on HGF-stimulated growth of MDA-MB-231, MDA-MB-468, and T-47D breast cancer cells after 72 h. Viable cell count was determined using MTT assay. Vertical bars indicate the mean cell count  $\pm$  SEM of N=3/dose.

**Figure 8.** In silico binding mode of **HVS-16** at the ATP binding site of c-Met kinase domain. (A) Overview of **HVS-16**'s binding pose at the c-Met crystal structure 3F82. (B) Important interactions of **HVS-16** at the c-Met crystal structure 3F82. (C) Important interactions of **HVS-16** at the c-Met crystal structure 4XYF. (D) Structure overlay for **HVS-16** (tube) with ligand **49** conformations (thin tube) obtained from c-Met crystal structure 3F82 and from a docking simulation. (E) *Left panel*, in silico binding pose of **HVS-16** at the ATP binding site of the c-Met kinase domain (PDB 4XYF) to show the U-shape conformation; *Right panel*, the

transparent protein surface, in aquamarine color, and the solid **HVS-16** surface, in yellow green color, are shown to emphasize the **HVS-16**'s shape fitting within the target pocket.

**Table 1.** c-Met inhibitory activity of compounds **1-47** in Z'-LYTE™ kinase assay.

<b>Compound</b>	<b>IC<sub>50</sub> (μM) ± SEM</b>
<b>1</b>	5.2 ± 0.4
<b>2</b>	>20
<b>3</b>	>20
<b>4</b>	13.7 ± 0.6
<b>5</b>	12.9 ± 0.2
<b>6</b>	20.2 ± 0.5
<b>7</b>	>20
<b>8</b>	>20
<b>9</b>	>20
<b>10</b>	>20
<b>11</b>	>20
<b>12</b>	>20
<b>13</b>	5.8 ± 0.3
<b>14</b>	>20
<b>15</b>	7.8 ± 0.9
<b>16</b>	1.0 ± 0.2
<b>17</b>	1.3 ± 0.4
<b>18</b>	5.2 ± 0.3
<b>19</b>	6.1 ± 0.8
<b>20</b>	8.2 ± 0.8
<b>21</b>	9.1 ± 0.7
<b>22</b>	>20
<b>23</b>	>20
<b>24</b>	>20

Table 1. *Continued*

<b>Compound</b>	<b>IC<sub>50</sub> (μM) ± SEM</b>
25	>20
26	>20
27	>20
28	11.4 ± 0.9
29	7.6 ± 0.9
30	8.5 ± 1.2
31	>20
32	8.3 ± 1.1
33	1.2 ± 0.1
34	>20
35	8.0 ± 0.2
36	>20
37	6.9 ± 0.3
38	12.2 ± 0.3
39	2.1 ± 0.1
40	>20
41	2.3 ± 0.5
42	3.2 ± 0.4
43	3.5 ± 0.5
44	1.1 ± 0.4
45	1.2 ± 0.8
46	5.8 ± 1.2
47	5.3 ± 0.2

**Table 2.** Antiproliferative and antimigratory activities of compounds **1-47** against TNBC human breast cancer cell lines in 2D monolayer cultures.

Compound	Antiproliferative activity		Antimigratory activity
	IC <sub>50</sub> (μM) ± SEM		IC <sub>50</sub> (μM) ± SEM
	MDA-MB-231	MDA-MB-468	MDA-MB-231
<b>1</b>	15 ± 1.4 <sup>a</sup>	19.1 ± 1.2	7.5 ± 1.1
<b>2</b>	80.4 ± 2.1	93.7 ± 1.5	13.8 ± 0.6
<b>3</b>	>100	>100	>50
<b>4</b>	79.5 ± 1.1	88.8 ± 1.4	33.5 ± 0.9
<b>5</b>	87.6 ± 0.9	95.5 ± 1.9	44.3 ± 4.3
<b>6</b>	59.9 ± 2.3	64.2 ± 2.1	30.5 ± 3.2
<b>7</b>	91.3 ± 3.1	92.2 ± 1.1	>50
<b>8</b>	83.2 ± 1.1	89.2 ± 1.4	40.6 ± 5.1
<b>9</b>	68.8 ± 2.1	74.5 ± 0.9	30.4 ± 1.1
<b>10</b>	72.8 ± 0.6	80.2 ± 0.6	>50
<b>11</b>	89.9 ± 2.1	91.1 ± 1.9	4.6 ± 0.6
<b>12</b>	72.3 ± 0.7	79.1 ± 1.3	16.3 ± 2.2
<b>13</b>	18.9 ± 0.3	21.1 ± 0.7	4.2 ± 1.9
<b>14</b>	16.0 ± 3.2	20.3 ± 1.1	12.7 ± 1.7
<b>15</b>	12.7 ± 2.8	14.2 ± 2.1	4.5 ± 1.3
<b>16</b>	3.8 ± 0.8	6 ± 0.7	2.5 ± 0.5
<b>17</b>	10.5 ± 0.4	13.3 ± 0.9	4.6 ± 0.3
<b>18</b>	13.0 ± 1.4	15.2 ± 1.2	7.5 ± 1.0
<b>19</b>	10.1 ± 1.2	14.1 ± 1.9	5.6 ± 0.8
<b>20</b>	7.6 ± 1.5	9.4 ± 1.1	4.8 ± 0.4
<b>21</b>	4.4 ± 1.3	7.4 ± 1.4	4.1 ± 0.8
<b>22</b>	10.6 ± 1.1	14.2 ± 1.2	8.3 ± 1.7
<b>23</b>	11.8 ± 0.9	15.9 ± 0.3	8.1 ± 1.4
<b>24</b>	7.3 ± 0.5	8.9 ± 1.5	5.4 ± 2.1

<sup>a</sup> Consistent with the reported IC<sub>50</sub> of **1** in MTT assay [20].

Table 2. *Continued*

Compound	Antiproliferative activity		Antimigratory activity
	IC <sub>50</sub> (μM) ± SEM		IC <sub>50</sub> (μM) ± SEM
	MDA-MB-231	MDA-MB-468	MDA-MB-231
25	8.2 ± 2.1	9.9 ± 1.3	6.2 ± 2.2
26	9.2 ± 2.3	8.6 ± 1.4	7.8 ± 0.6
27	10.1 ± 0.7	10.5 ± 0.9	8.1 ± 1.4
28	8.6 ± 0.6	10.1 ± 2.3	5.2 ± 0.5
29	12.2 ± 0.4	15.5 ± 2.1	11.8 ± 1.1
30	14.7 ± 1.1	17.2 ± 1.7	13.3 ± 0.6
31	27.9 ± 0.8	31.2 ± 1.2	18.8 ± 2.1
32	25.3 ± 0.6	27.6 ± 1.4	21.6 ± 4.1
33	10.3 ± 1.1	13.2 ± 1.6	4.1 ± 1.4
34	17.4 ± 0.2	19.1 ± 1.3	>50
35	15.8 ± 1.2	16.1 ± 1.8	4.3 ± 0.6
36	19.3 ± 2.1	23.4 ± 1.2	8.7 ± 0.7
37	9.2 ± 2.2	10.4 ± 1.4	4.6 ± 1.2
38	40.5 ± 1.4	46.2 ± 2.4	31.2 ± 0.8
39	4.2 ± 0.4	6.9 ± 1.2	4.0 ± 0.7
40	22.3 ± 3.2	25.6 ± 0.9	19.8 ± 1.1
41	6.3 ± 1.5	8.2 ± 0.5	5.4 ± 3.2
42	13.7 ± 0.7	17.2 ± 0.9	8.2 ± 0.7
43	15.1 ± 1.2	16.8 ± 1.1	9.3 ± 0.2
44	9.3 ± 0.8	10.7 ± 1.5	3.6 ± 0.2
45	9.5 ± 0.6	11.5 ± 1.2	3.9 ± 0.9
46	15.4 ± 2.2	15.9 ± 0.3	14.2 ± 3.2
47	13.3 ± 0.9	17.6 ± 0.7	12.6 ± 2.3

**Table 3.** Anti-invasive activity of analogs **16**, **21** and **39** against the highly metastatic MDA-MB-231 human breast cancer cell line. Meanwhile, compounds **1** and **4** were used as positive standard controls and their IC<sub>50</sub> values were calculated for activity comparison.

Compound	Anti-invasive activity
	IC <sub>50</sub> (μM) ± SEM
	<b>MDA-MB-231</b>
<b>1</b>	18.2 ± 1.6
<b>4</b>	19.8 ± 1.1
<b>16</b>	2.7 ± 0.8
<b>21</b>	14.2 ± 0.6
<b>39</b>	7.1 ± 0.7

## LIST OF ABBREVIATIONS

c-Met, mesenchymal-epithelial transition factor; SAR, structure-activity relationship; RTK, receptor tyrosine kinase; RON, recepteur d'origine Nantais; HGF, hepatocyte growth factor; EGFR, epidermal growth factor receptor; BRAF, v-RAF murine sarcoma viral oncogene homolog B1; ALK, anaplastic lymphoma receptor tyrosine kinase; VEGFR, vascular endothelial cell growth factor receptor; NSCLC, non-small cell lung cancer; EVOO, extra-virgin olive oil; Hsp90, heat shock protein 90; HER2, human epidermal growth factor receptor 2; ATP, adenosine triphosphate; GST, glutathione S-transferase; HRESIMS, high-resolution electron spray ionization mass spectrometry; PENDANT, polarization enhancement during attached nucleus testing; HMBC, heteronuclear multiple bond correlation; MTT, 3-[4,5-dimethylthiazol-2-yl]-2,5-diphenyltetrazolium bromide; WHA, wound-healing assay; TNBC, triple-negative breast cancer; BME, basement membrane extract; 3D, three-dimensional; 2D, two-dimensional; IC<sub>50</sub>, 50% inhibitory concentration; HBD, hydrogen bond donor; HBA, hydrogen bond acceptor; HB, hydrogen bond; Å, Angstrom; PDB, protein data bank; DMSO, dimethyl sulfoxide; ERα, Estrogen receptor α; RMSD, root mean square displacement; TLC, thin layer chromatography; EtOAc, ethyl acetate; CDCl<sub>3</sub>, deuterated chloroform; TMS, tetramethylsilane; TPP, triphenylphosphine; THF, tetrahydrofuran; DIAD, diisopropylazodicarboxylate; TEA, triethylamine; DMF, dimethylformamide; BOP, benzotriazol-1-yloxy-tris phosphonium hexafluoro phosphate; CH<sub>2</sub>Cl<sub>2</sub>, dichloromethane; MeOH, methanol; EDCI, 1-ethyl-3-(3-dimethylaminopropyl) carbodiimide; FBS, fetal bovine serum; EGF, epidermal growth factor; PBS, phosphate buffer saline; AM, acetomethyl ester; RFU, relative fluorescence units; SDS, sodium dodecyl sulfate; PVDF, polyvinylidene fluoride; BSA, bovine serum albumin; TBST, tris-buffered saline with Tween 20; OPLS, optimized potentials for liquid simulation; XP, extra-precision; SEM, standard error of a mean; ANOVA, analysis of variance.

Figure. 1

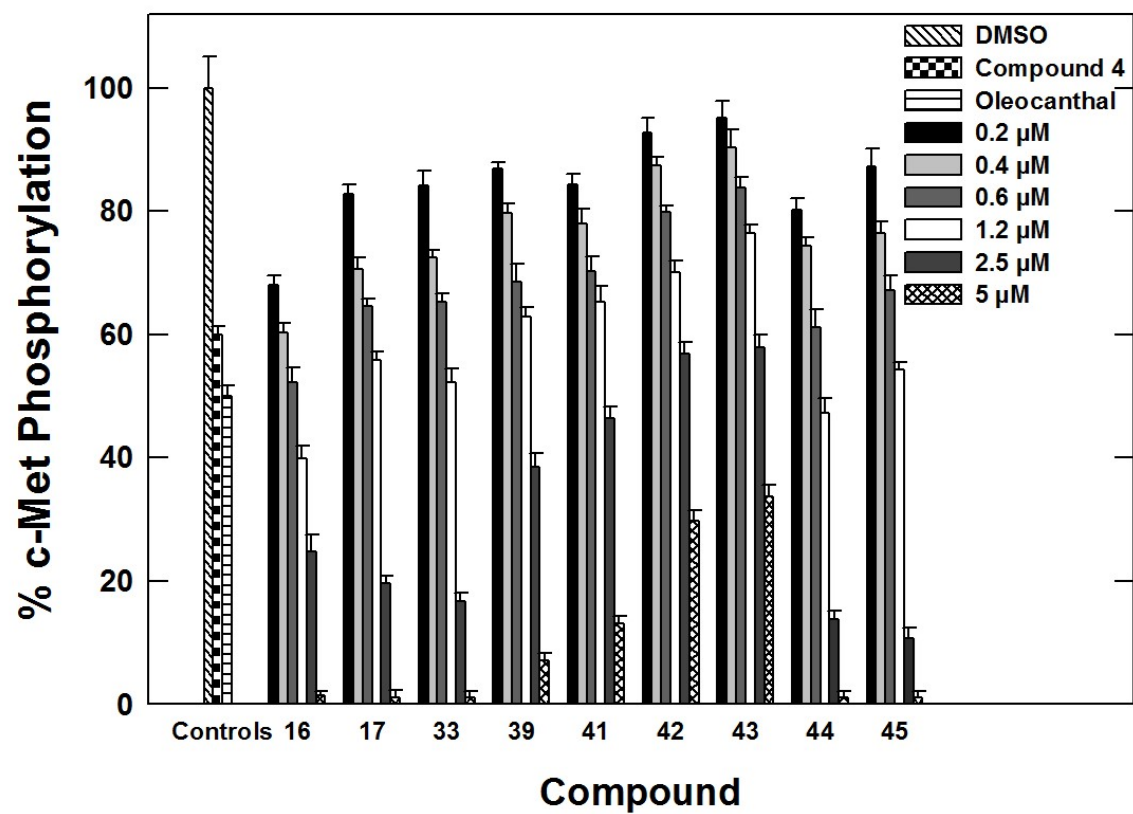


Figure. 2

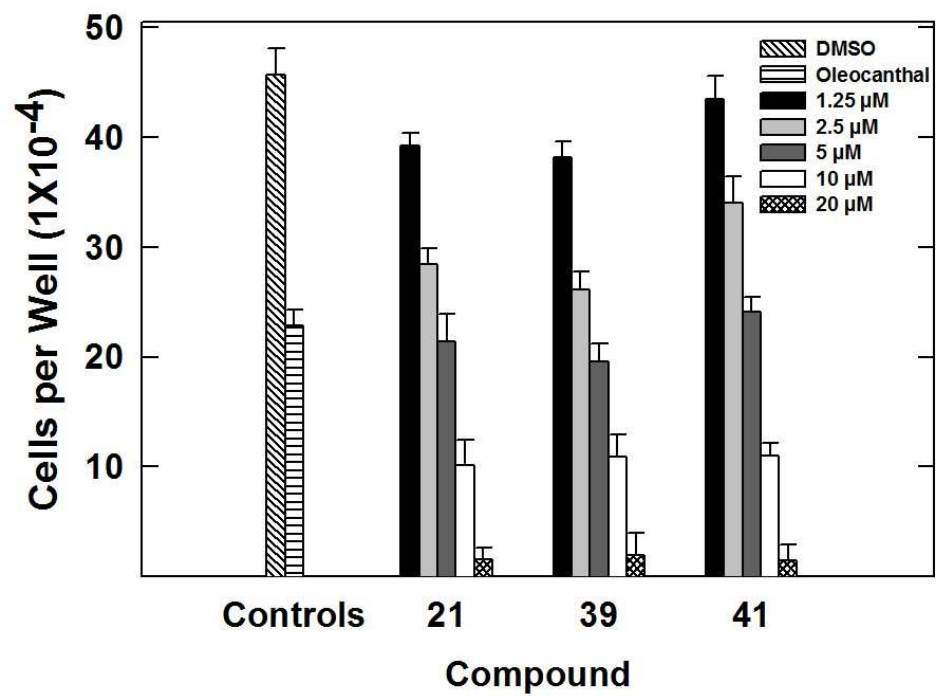
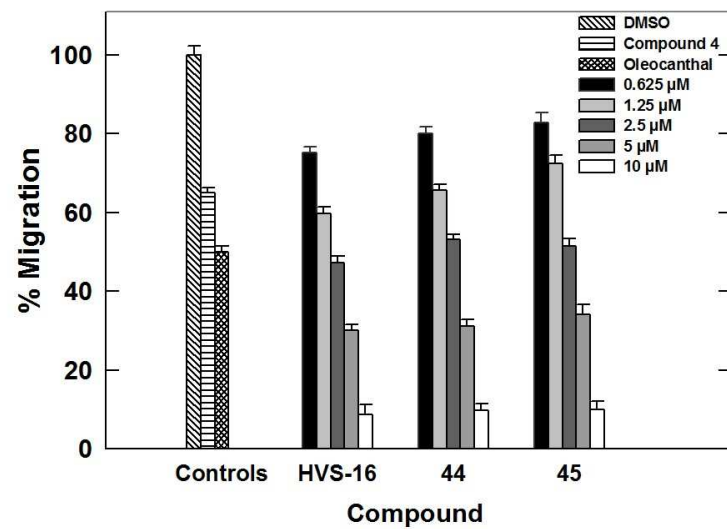


Figure. 3

A



B

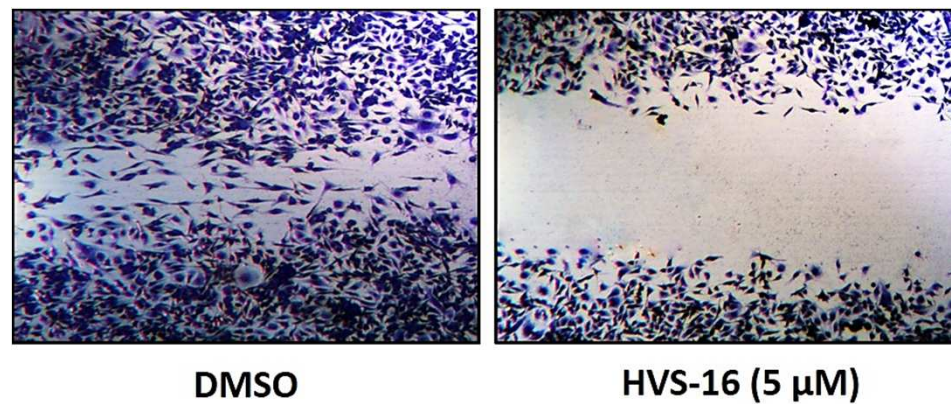


Figure. 4

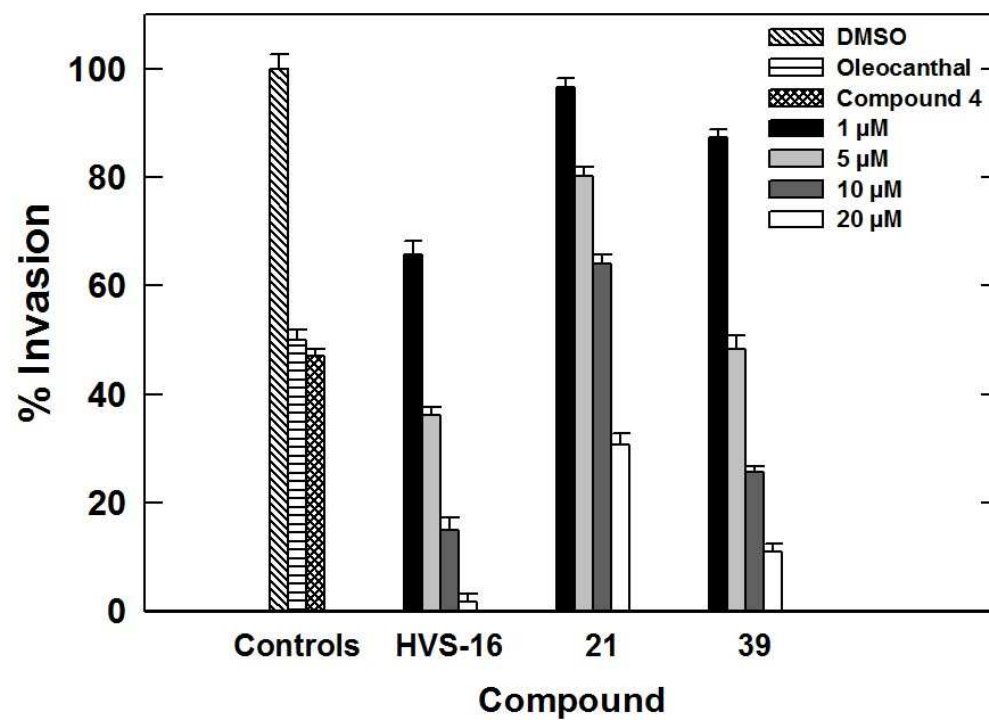


Figure. 5

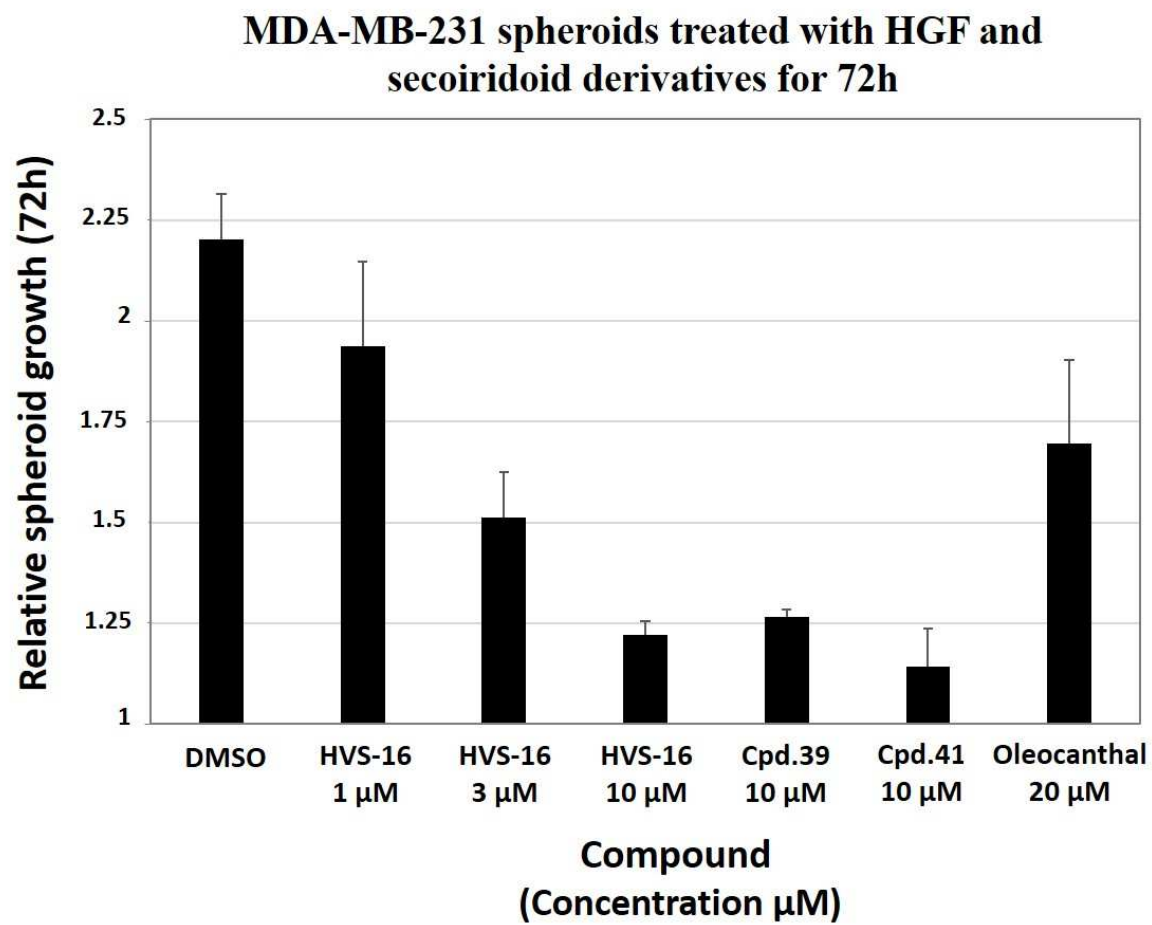


Figure. 6

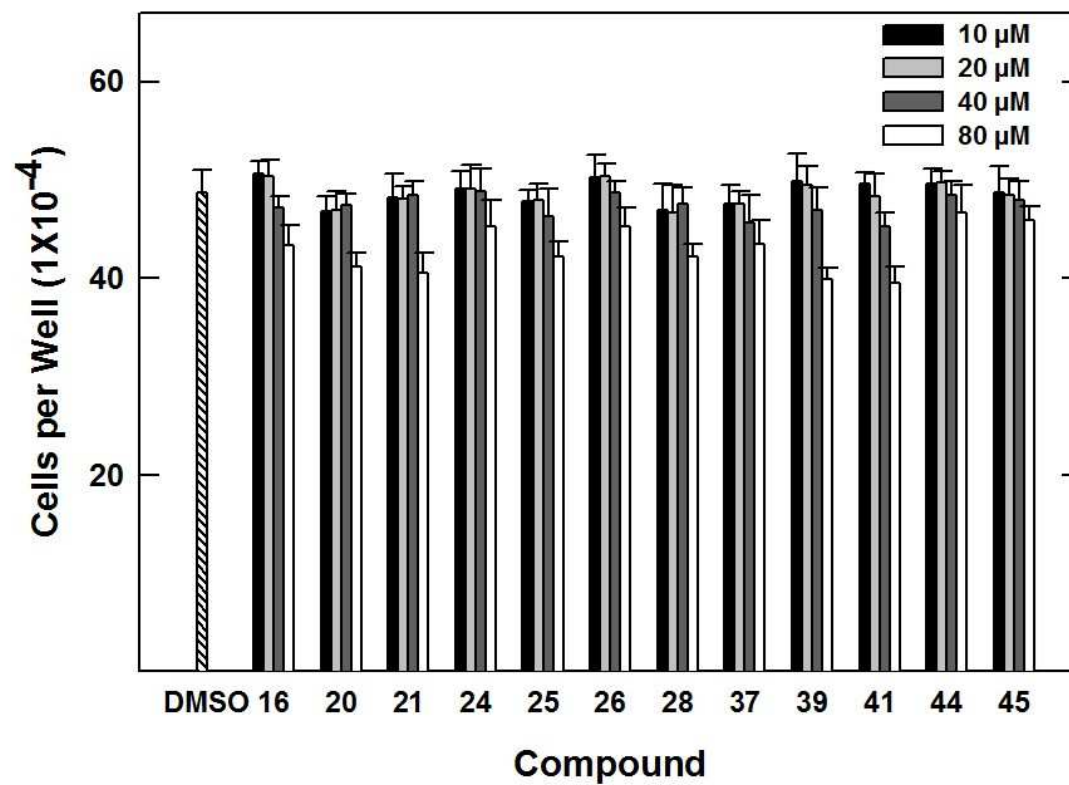
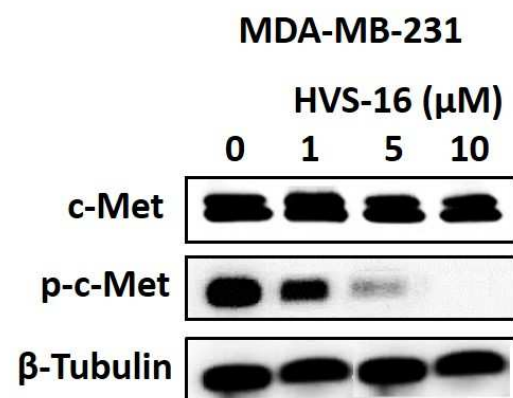


Figure. 7

A



B

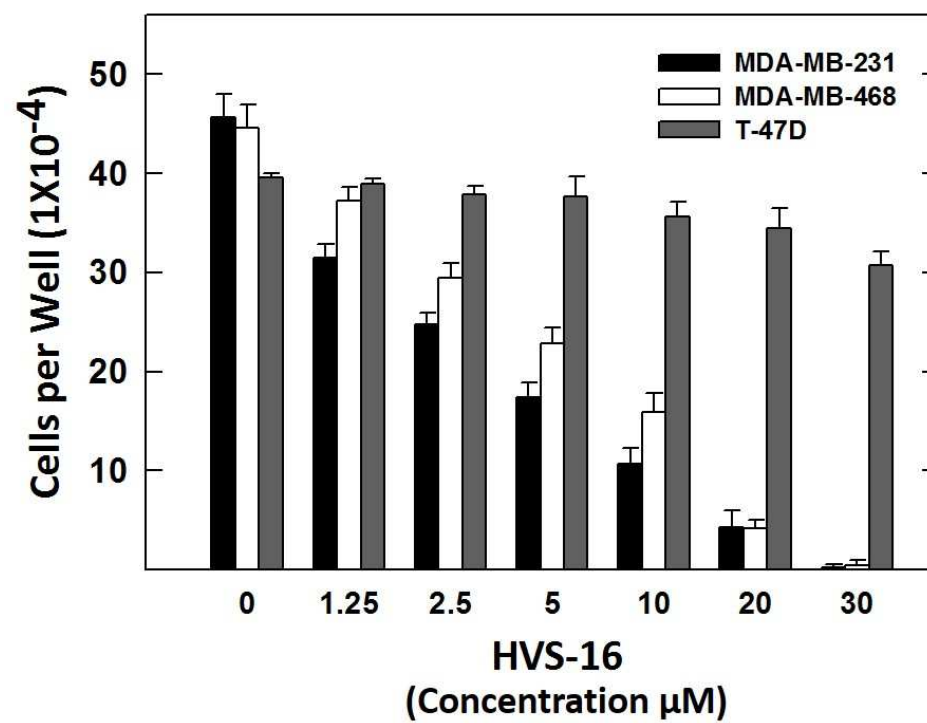


Figure. 8

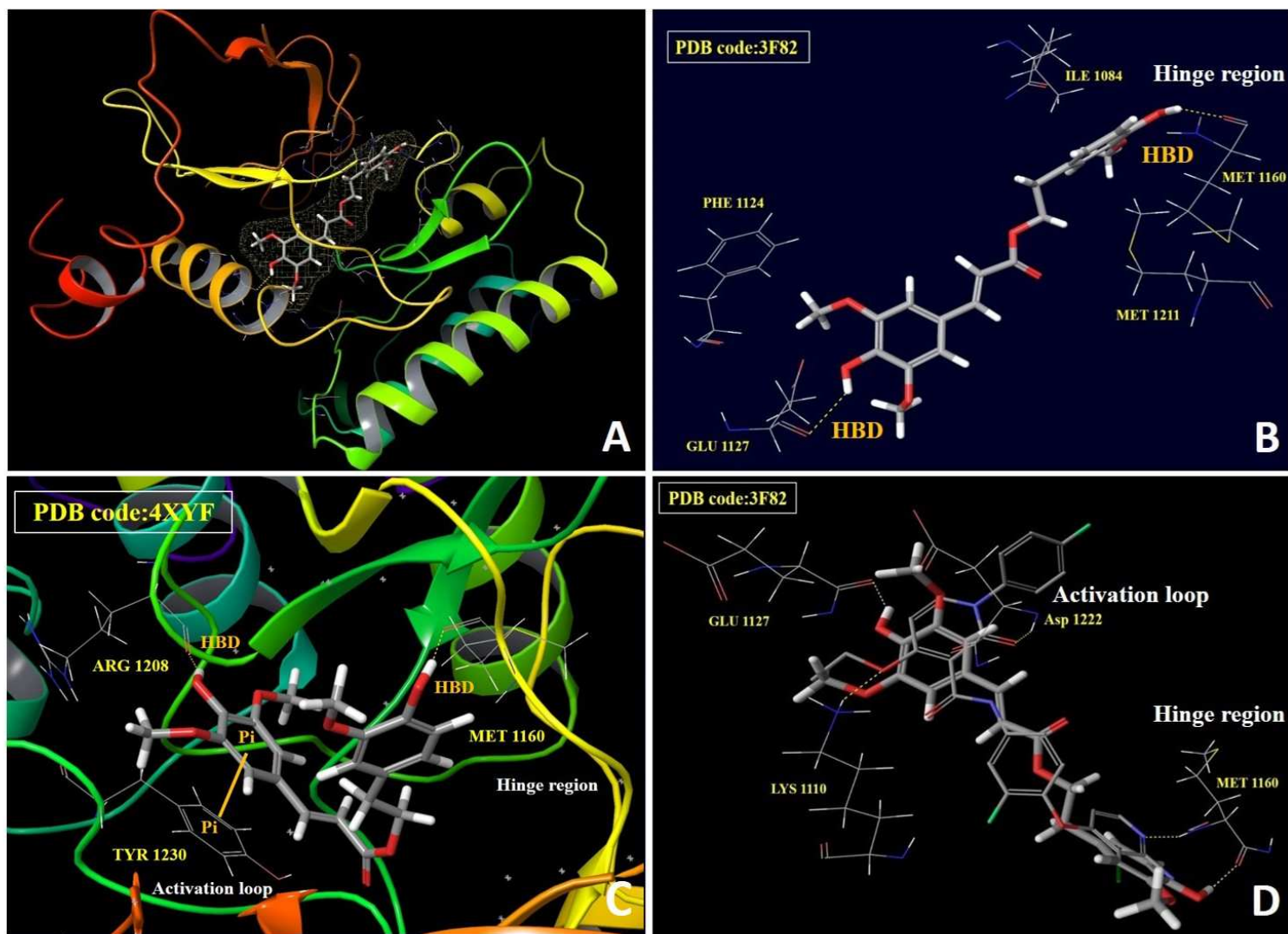
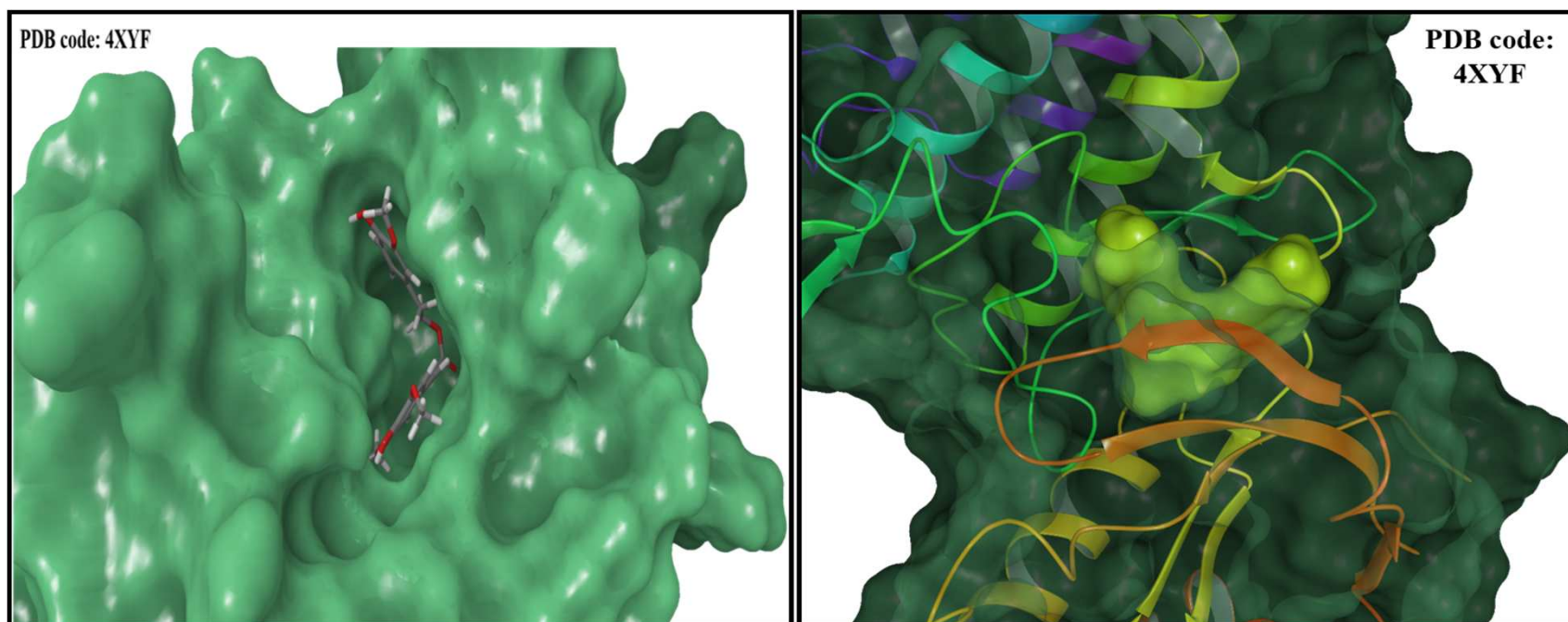


Figure. 8E



## Highlights

- Inspired by (-)-oleocanthal, **HVS-16** was discovered as a novel c-Met inhibitor hit.
- **HVS-16** impaired Met-mediated cellular events across 2D & 3D breast cancer cultures.
- **HVS-16** had no effect on both non-cancerous and Met-independent breast cancer cells.
- Inhibition of c-Met activation was confirmed by Western blot and docking studies.